CrossMark

Distributed vortex receptivity of a swept-wing boundary layer. Part 2. Receptivity characteristics

V. I. Borodulin[1], A. V. Ivanov[1], Y. S. Kachanov[1],† and A. P. Roschektayev[1]

[1]Khristianovich Institute of Theoretical and Applied Mechanics SB RAS, Institutskaya str. 4/1,
Novosibirsk 630090, Russia

This paper is devoted to an experimental investigation of the distributed receptivity of a laminar swept-wing boundary layer to unsteady freestream vortices with streamwise orientation of the vorticity vector. The experiments were performed on a model of a swept wing with a sweep angle of $25°$ at fully controlled disturbance conditions with freestream vortices generated by a special disturbance source. It is found that the unsteady streamwise vortices are able to provide very efficient excitation of cross-flow instability modes without requiring the presence of any surface non-uniformities. The developed experimental approach is shown to allow us to perform a detailed quantitative investigation of the mechanism of distributed excitation of unsteady boundary-layer disturbances due to scattering of freestream vortices on natural base-flow non-uniformity. This mechanism has been studied experimentally in detail. Part 1 of the present investigation (Borodulin *et al.*, *J. Fluid Mech.*, vol. 908, 2021, A14) was devoted to the description of the experimental approach and the base-flow structure, the method of excitation of fully controlled streamwise-elongated freestream vortices, the results of measurements of structure of these vortices and the experimental evidence of high efficiency of the distributed vortex receptivity mechanism under study. Meanwhile, the present paper (Part 2) is devoted to: (a) theoretical background and definition of the distributed receptivity coefficients and (b) obtaining experimental quantitative characteristics of the distributed vortex receptivity including values of the corresponding receptivity coefficients for their three different definitions as functions of the disturbance frequency, spanwise wavenumber and wave propagation angle.

Key words: boundary-layer receptivity, boundary-layer stability, transition to turbulence

1. Introduction

A detailed introduction, including a description of the motivation of the present work, has been given in Part 1 of the present study (see Borodulin *et al.* 2021). The present paper (Part 2) is devoted to very deep processing and analysis of the experimental data. Several stages of this rather complicated analysis are briefly described in the abstract.

† Email address for correspondence: kachanov@itam.nsc.ru

The experiments discussed in the present two-part paper were carried out in as early as 2002 within the framework of a research contract between the Khristianovich Institute of Theoretical and Applied Mechanics (ITAM) SB RAS and the Boeing Operations International, Inc., but were only previously published in technical reports (Kachanov *et al.* 2002*a,b*) and, very briefly, in the proceedings of a conference (Borodulin, Ivanov & Kachanov 2010*a,b*).

The experiments were conducted in a low-turbulence subsonic wind tunnel T-324 of ITAM. Two sets of measurements were performed simultaneously in a swept-wing boundary layer, which was simulated on a swept flat plate having elliptic leading edge: (i) the distributed receptivity (DR) experiments and (ii) the stability (S) experiments. The chordwise pressure gradient was induced by a contoured wall bump (uniform in the spanwise direction) mounted on the test-section ceiling just above the swept plate. Both the plate and the bump had the same sweep angle $\chi = 25°$. The experimental model was equipped with two contoured sidewalls in order to diminish the influence of the wind-tunnel test-section walls and to provide better satisfaction of the sweep condition. The freestream turbulence level (in the frequency range higher than 1 Hz) was approximately 0.06 % under the present experimental conditions. All main measurements were carried out by means of the hot-wire anemometer.

The characteristics of the three-dimensional mean flow field over the present experimental model were measured in detail in both the potential flow and the boundary layer using, in particular, V-shaped hot-wire probes. These measurements were carried out in previous experiments. The results of these measurements were described by Borodulin *et al.* (2013, 2016). Additional information about the mean flow characteristics observed under the conditions of the present set of measurements was presented by Borodulin *et al.* (2021).

The main coordinate systems used in the present experiments are as follows. The (x, z) system is connected to the incident flow-velocity direction (upstream of the model) with the mean velocity vector C_o parallel to the x-axis. The x'-axis is directed along the chord and starts at the leading edge of the model. The z'-axis is parallel to the leading edge. The (x^*, z^*) coordinate system is local, such that the x^*-axis is directed along the local mean velocity vector C_e of the potential flow near the external edge of the boundary layer. It is also convenient to use an additional axis x_c, which is parallel to the x-axis but always has its origin on the swept-plate leading edge, as well as an additional axis z'_c, which is similar to the z'-axis but always has its origin at the model centreline, that is, at $z = 0$.

2. Methods of experimental determination of DR functions

2.1. *Analytical solutions used for approximation of cross-flow-wave behaviour*

Note, first, that during the DR analysis described below in § 2, the x' coordinate is counted (for simplicity) from the first measured section at $x' = 438.2$ mm, that is, x' is regarded to be equal to zero at this first point.

Similar to experiments by Würz *et al.* (2002) and Borodulin *et al.* (2006, 2007), let us consider the distributed generation of cross-flow (CF) waves in a swept-wing boundary layer by three-dimensional (in general) freestream vortices, which are periodic in time and represent a kind of three-dimensional vortex street. Both the CF wave and the vortex street have a certain fixed real frequency $\omega = 2\pi f$ and a certain fixed real spanwise wavenumber β'. It is convenient to present the perturbation of the streamwise velocity component,

associated with the generated CF wave, as

$$\bar{u}^d(x', y, z', t) = \bar{B}^d(x', y) \exp\left[i\left(\beta'z' - \omega t\right)\right],\tag{2.1}$$

where $\bar{B}^d(x', y)$ is the complex-valued CF wave amplitude. (All complex functions are marked here with overbars, as vectors.) Similarly, the perturbation of the streamwise velocity component, associated with the freestream vortex street, is convenient to present as

$$\bar{u}_v(x', y, z', t) = \bar{B}_v(x', y) \exp\left[i\left(\beta'z' - \omega t\right)\right],\tag{2.2}$$

where $\bar{B}_v(x', y)$ is the complex-valued freestream vortex amplitude.

Total change of the velocity perturbation, associated with boundary-layer disturbance $d\bar{u}^d(x', y, z', t)$ excited within an infinitely small interval dx' of the chordwise coordinate (around the x' position) is

$$d\bar{u}^d(x', y_m, z', t) = d\bar{u}_s(x', y_m, z', t) + d\bar{u}_r(x', y_m, z', t),\tag{2.3}$$

where $d\bar{u}_s(x', y_m, z', t)$ is a portion of the change that occurred due to the boundary-layer instability (i.e. owing to the evolution of the previously generated boundary-layer disturbance), $d\bar{u}_r(x', y_m, z', t)$ is a portion of change due to the DR (i.e. an additionally generated portion of the boundary-layer disturbance) and y_m is a certain wall-normal distance, which corresponds to the maximum amplitude of the boundary-layer disturbance with frequency f and spanwise wavenumber β' (y_m, of course, depends, in general, also on the x' coordinate). For functions $d\bar{u}_s(x', y_m, z', t)$ and $d\bar{u}_r(x', y_m, z', t)$, we have

$$d\bar{u}_s(x', y_m, z', t) = i\bar{\alpha}'(x')\bar{u}^d(x', y_m, z', t)\, dx' = i\bar{\alpha}'(x')\bar{B}^d(x', y_m) \exp[i(\beta'z' - \omega t)]\, dx',\tag{2.4}$$

where

$$\bar{\alpha}'(x') = \alpha_r'(x') + i\alpha_i'(x')\tag{2.5}$$

is the complex-valued streamwise wavenumber of the excited CF instability modes (i.e. the eigenvalues of the corresponding linear stability problem) and

$$d\bar{u}_r(x', y_m, z', t) = \bar{u}_v(x', y, z', t)\,|_{y=\delta}\, \bar{G}_v^d(x')\, dx'$$
$$= \bar{B}_v(x', y)\,|_{y=\delta}\, \exp[i(\beta'z' - \omega t)]\bar{G}_v^d(x')\, dx',\tag{2.6}$$

where δ is the boundary-layer thickness and $\bar{G}_v^d(x')$ is the complex-valued distributed vortex receptivity function. Equation (2.6) can be regarded as one of possible definitions of this function.

Substitution of (2.4) and (2.6) into (2.3) gives us the main equation, which connects all three complex-valued functions (the boundary-layer wave amplitude, the freestream vortex amplitude and the receptivity function):

$$\frac{d\bar{B}^d(x', y_m)}{dx'} = i\bar{\alpha}'(x')\bar{B}^d(x', y_m) + \bar{B}_v(x', y)\,|_{y=\delta}\, \bar{G}_v^d(x').\tag{2.7}$$

This equation describes streamwise evolution of the boundary-layer disturbances excited in a distributed way by freestream vortices.

Equation (2.7) can be also regarded as another possible definition of the distributed vortex receptivity function $\bar{G}_v^d(x')$.

It is important to note here that the evolutionary equation (2.7) is a result of a significant simplification of the mechanism of distributed excitation of the CF instability waves, which (i) ignores the disturbance-source near-field, (ii) assumes that the CF modes are excited in the boundary layer directly by the freestream vortices and (iii) assumes that the base-flow non-parallelism does not change dramatically the DR mechanism under study. However, such simplification seems to be reasonable because every newly excited portion of the boundary-layer disturbances is rather weak and does not perturb strongly either the previously excited CF waves or the bounded disturbances associated with the freestream vortices present at the boundary-layer edge. The application of such an evolutionary equation performed in several previous studies, as well as in the present work, for approximation of the experimentally observed disturbance fields corroborates the correctness of such simplification and its applicability to extracting the receptivity coefficients from the experimental data. The procedure of such extraction is the only goal of application of (2.7) in the DR experiments. This equation is not intended for solving theoretical problems.

Let us assume now that we know from experiment all functions included in (2.7) except for the receptivity function $\bar{G}_v^d(x')$, which has to be found. The latter can be expressed explicitly in the following way:

$$\bar{G}_v^d(x') = \frac{\boldsymbol{L}\{\bar{B}^d(x', y_m)\}}{\bar{B}_v(x', y)\mid_{y=\delta}}, \tag{2.8}$$

where

$$\boldsymbol{L} = \frac{\mathrm{d}}{\mathrm{d}x'} - \mathrm{i}\bar{\alpha}'(x'), \tag{2.9}$$

is a linear operator. Equations (2.8) and (2.9) can be also regarded as a definition of the DR function $\bar{G}_v^d(x')$. It is seen that the most significant difference between the localised receptivity function (which could be defined in a hypothetical case of a localised vortex positioned permanently at the fixed streamwise coordinate x')

$$\bar{G}_v(x') = \frac{\bar{B}(x', y_m)}{\bar{B}_v(x', y)\mid_{y=\delta}}, \tag{2.10}$$

and the DR function (2.8) is the presence of operator $\boldsymbol{L}$, which indicates that the DR is essentially a local, differential boundary-layer characteristic, which describes a derivative of the disturbance amplitude, that is, the growth of CF waves additional to the linear-stability growth, whereas the usual, localised receptivity is responsible for the generation of a certain amplitude of the CF wave occurring in the point x'.

To find the DR coefficients in experiment, the method of approximation of streamwise distributions of measured normal-mode amplitudes and phases by analytical solutions was used. For two-dimensional boundary layers, this method is described and used by Borodulin *et al.* (2006, 2007).

Keeping in mind that the wall-normal coordinates are fixed (as shown in (2.7)), let us assume now that $\bar{\alpha}'(x') = \alpha'_r + \mathrm{i}\alpha'_i = \mathrm{const.}$ and $\bar{B}_v(x') = B_{vo}\exp[\mathrm{i}(\bar{\alpha}'_v x' + \phi_{vo})]$, where B_{vo}, α'_v and ϕ_{vo} are constants, and $\bar{G}_v^d(x') = G_{vo}^d\exp[\mathrm{i}(\bar{\alpha}'_g x' + \lambda_{vo}^d)]$, where G_{vo}^d, $\bar{\alpha}'_g$ and λ_{vo}^d are constants. This can be close to reality if the chordwise range of main receptivity measurements is not very long. In this case (2.7) has rather simple analytical solutions. Let us find them.

It is convenient to introduce, first, the following values: $\bar{\alpha}'_{gv} = \bar{\alpha}'_g + \bar{\alpha}'_v$ and $\phi_{gvo} = \lambda^d_{vo} + \phi_{vo}$. Let us also introduce a resonance detuning of the complex-valued streamwise wavenumbers as $\bar{\sigma}' = \sigma'_r + i\sigma'_i = \bar{\alpha}'_{gv} - \bar{\alpha}'$. The solutions of (2.7) are different in the non-resonant ($\bar{\sigma}' \neq 0$) and resonant ($\bar{\sigma}' = 0$) cases. In the non-resonant case the solution is

$$\bar{B}^d(x') = B_{1o} \exp[i(\bar{\alpha}'x' + \phi_{1o})] + \frac{G^d_{vo}B_{vo}}{i\bar{\sigma}'} \exp[i(\bar{\alpha}'x' + \phi_{gvo})] \exp(i\bar{\sigma}'x'). \quad (2.11)$$

Here the first term on the right-hand side is a 'pure' CF mode developing in the absence of freestream vortices, whereas the second term is a bounded (forced) mode associated with the distributed excitation of the boundary-layer disturbances. Note that (2.11) remains valid when $\sigma'_r = 0$ (the resonance of streamwise wavenumbers) or $\sigma'_i = 0$ separately. Meanwhile, when $\bar{\sigma}' = 0$ (i.e. $\sigma'_r = \sigma'_i = 0$) we have the true resonant case, the solution for which is

$$\begin{aligned}\bar{B}^d(x') &= B^d_o \exp[i(\bar{\alpha}'x' + \phi^d_o)] + G^d_{vo}B_{vo} \exp[i(\bar{\alpha}'x' + \phi_{gvo})]x' \\ &= (\bar{B}^d_o + \bar{G}^d_{vo}\bar{B}_{vo}x') \exp(i\bar{\alpha}'x'), \end{aligned} \quad (2.12)$$

where $\bar{B}^d_o$, $\bar{G}^d_{vo}$ and $\bar{B}_{vo}$ are complex-valued initial amplitudes of the boundary-layer disturbance, of the receptivity function and of the freestream vortex, respectively. In this resonant solution, the pure CF mode and the bounded (forced) mode become indistinguishable and the excited disturbance growth corresponds to the exponential growth (as that of the pure CF mode) but with linearly growing 'initial' magnitude. Equation (2.12) indicates that even if the pure CF mode attenuates downstream, the mechanism of the resonant distributed vortex receptivity is able to lead to its amplification in a certain initial range of the chordwise coordinate. This behaviour is similar to the 'transient' growth observed in bypass transition scenarios, but in the present case this transient growth is associated exclusively with the distributed vortex receptivity mechanism. Note also that the *N*-factor methods of transition prediction cannot be applied (directly) in this case.

Let us assume now that

$$\bar{G}^d_v(x') = \bar{G}^d_{vo} = G^d_{vo} \exp(i\lambda^d_{vo}) \quad (2.13)$$

is independent of the streamwise coordinate, that is, G^d_{vo} and λ^d_{vo} are constants. This assumption is reasonable if the chordwise range of the main receptivity measurements is very short. In this case, the general solution of (2.7) is simplified and instead of (2.11) we have

$$\bar{B}^d(x') = B_{1o} \exp[i(\bar{\alpha}'x' + \phi_{1o})] + \frac{G^d_{vo}B_{vo}}{i\bar{\sigma}'} \exp[i(\bar{\alpha}'_v x' + \phi_{gvo})], \quad (2.14)$$

where the resonance detuning of the complex-valued streamwise wavenumbers is also simplified now as $\bar{\sigma}' = \bar{\alpha}'_v - \bar{\alpha}'$, $\bar{B}_{1o}$ and $\bar{B}_{vo}$ are complex-valued initial amplitudes of the boundary-layer disturbance and the freestream vortex, respectively. This solution is valid for non-resonant cases, when $\bar{\sigma}' \neq 0$. Our measurements have shown that $\bar{\sigma}'$ becomes very rarely close to zero in all studied cases under the assumption of constancy of the DR coefficients (2.13). Note also that solution (2.14) remains valid when either $\sigma'_r = 0$ (the resonance of real streamwise wavenumbers) or $\sigma'_i = 0$ separately.

2.2. *Procedures of approximation and obtaining the DR coefficients*

The analytical solutions (2.11), (2.12) and (2.14) were used for approximation of experimental data during the procedure of obtaining the DR coefficients (see § 3).

In both the non-resonant and resonant cases the approximation was realised in 'MS Excel' files using the MS Excel Solver. The solver minimised the root-mean-square deviation of the distance between the measured ($\bar{B}^d_{exp}(x')$) and approximated ($\bar{B}^d_{apr}(x')$) values of complex-valued boundary-layer disturbance amplitudes in a complex plane. This deviation was calculated as

$$\Delta B^d_{rel} = \frac{\sqrt{\overline{\overline{\delta B^d(x')^2}}}}{\overline{\overline{\delta B^d_m(x')}}}, \tag{2.15}$$

where a double overbar means averaging for all points measured at various x' coordinates and

$$\delta B^d(x') = \left| \frac{\bar{B}^d_{exp}(x') - \bar{B}^d_{apr}(x')}{2} \right|, \quad \delta B^d_m(x') = \left| \frac{\bar{B}^d_{exp}(x') + \bar{B}^d_{apr}(x')}{2} \right|. \tag{2.16a,b}$$

Note that despite ΔB^d_{rel} representing a relative root-mean-square deviation, it is normalised by averaging in space disturbance amplitude rather than by amplitude in every particular spatial point. Therefore, the deviation minimised by the solver was, in fact, absolute. This was made with the purpose of diminishing the influence of small-amplitude points (where the experimental error was relatively large) on the approximation result.

2.3. *Notions of production function and efficiency function*

To better understand the DR mechanism, let us consider its efficiency depending on properties of the freestream vortices and of the excited CF waves.

As was mentioned in § 5.3 of Part 1 (Borodulin *et al.* 2021), as well as in other studies (see, e.g., Würz *et al.* 2002; Borodulin *et al.* 2006, 2007), some rather significant spatial beatings of spectral amplitudes and phases are observed in several spanwise-wavenumber ranges indicating to the presence of the distributed generation of instability waves. The beatings have spatial period

$$\Delta x'_b(x') = \frac{2\pi}{|\alpha'_{gr}(x') + \alpha'_{vr}(x') - \alpha'_r(x')|} = \frac{2\pi}{|\sigma'_r(x')|}. \tag{2.17}$$

In the case when the amplitudes of the DR function $G^d_v(x') = $ const. (i.e. $\alpha'_{gi} = 0$), the amplitude of the freestream vortex $B_v(x') = $ const. (i.e. $\alpha'_{vi} = 0$) and the amplitude of the excited CF wave $B(x') = $ const. (i.e. $\alpha'_i = 0$), the CF wave excited at the position x' will be completely cancelled by the CF wave excited at the position $x' + \Delta x'_b/2$. The CF wave excited at $x' + \Delta x'_b/2$ has the phase that is shifted by π with respect to the phase of the CF wave excited in the point x', whereas the amplitude of the newly excited portion is the same in this case. Therefore, the real averaged efficiency (the sense of this term is explained in the following) of the DR mechanism would be equal to zero when all three amplitude functions are constant (independently of the value of the DR coefficient G^d_v). Let us assume now that we still have $\alpha'_{vi} = 0$ and $\alpha'_i = 0$, but the receptivity amplitude function decreases with x' (i.e. $\alpha'_{gi} > 0$). In this case the CF wave excited at the position x' will be

cancelled only partially by the CF wave excited at the position $x' + \Delta x'_b/2$. The remaining difference $\Delta B^d(x')$ represents a CF wave, which is really excited by the distributed vortex receptivity mechanism integrally within one half of the period of beatings. This newly excited portion of CF wave can be characterised by a certain DR efficiency function $\Lambda(x')$ which is introduced in the following.

Under assumption that $\bar\alpha'_g$, $\bar\alpha'_v$ and $\bar\alpha'$ are independent of x' within the half-period of beatings $\Delta x'_b/2$, it is not difficult to show that the change of the CF wave amplitude $\mathrm{d}\bar B^d_\Delta$ appearing at step $\mathrm{d}x'$ owing to joint action of the DR mechanism and the instability mechanism can be expressed as

$$\mathrm{d}\bar B^d_\Delta = \bar B_v(x')\,|_{y=\delta}\; \bar G^d_v(x')\left\{\exp\left(\mathrm{i}\bar\alpha'\Delta x'\right) + \exp\left[\mathrm{i}\left(\bar\alpha'_v + \bar\alpha'_g\right)\Delta x'_b/2\right]\right\}\,\mathrm{d}x' = \bar P_\Delta\,\mathrm{d}x',\tag{2.18}$$

where the newly introduced function

$$\bar P_\Delta = P_\Delta \mathrm{e}^{\mathrm{i}(\phi_\Delta)}\tag{2.19}$$

is a kind of a production function, which characterises the efficiency of the DR mechanism in the sense described previously. This function can also be written in one of the following forms

$$\bar P_\Delta = B_v(x' + \Delta x'_b/2)G^d_v(x' + \Delta x'_b/2)\left[\mathrm{e}^{\pi\Lambda} - 1\right]\exp\left\{\mathrm{i}\left[\alpha_r\Delta x'_b/2 + \phi_v(x') + \lambda^d_v(x')\right]\right\}\tag{2.20}$$

for $\Lambda \geq 0$ and

$$\begin{aligned}\bar P_\Delta = B_v(x' + \Delta x'_b/2)G^d_v(x' + \Delta x'_b/2)\left[1 - \mathrm{e}^{\pi\Lambda}\right]\\ \times \exp\left\{\mathrm{i}\left[\phi_v(x' + \Delta x'_b/2) + \lambda^d_v(x' + \Delta x'_b/2)\right]\right\}\end{aligned}\tag{2.21}$$

for $\Lambda \leq 0$. Here

$$\Lambda = \frac{(\alpha'_{gi}) + (\alpha'_{vi}) - (\alpha'_i)}{|\alpha'_{gr}(x') + \alpha'_{vr}(x') - \alpha'_r(x')|} = \frac{\sigma'_i}{|\sigma'_r|}\tag{2.22}$$

is the efficiency function mentioned previously.

Equations (2.20), (2.21) clearly show the physical sense of the efficiency function Λ. The efficiency of the CF wave production by means of the distributed vortex receptivity mechanism depends essentially on the sign of function Λ. If $\Lambda = 0$, then $P_\Delta = 0$ and the production is absent. This means that the portion of CF wave generated in the point x' (and amplified downstream due to the linear instability mechanism) is completely cancelled in the point $x' + \Delta x'_b/2$ by another portion, which is newly generated in the vicinity of the point $x' + \Delta x'_b/2$.

If the efficiency function is positive ($\Lambda > 0$, (2.20)) the newly produced (at the point $x' + \Delta x'_b/2$) portion of the CF wave cancels the previous portion (produced at the point x') only partially. The remaining CF wave characterises an integral production of the instability wave within the distance $\Delta x'_b/2$. The phase of the remaining portion of disturbance $[\alpha_r\Delta x'_b/2 + \phi_v(x') + \lambda^d_v(x')]$ corresponds to the phase of the CF wave excited in the point x' (i.e. to the phase $[\phi_v(x') + \lambda^d_v(x')]$), which has been increased by the value of $\alpha'_r\Delta x'$ according to the linear stability behaviour. Thus, the resulting disturbance observed in the boundary layer at $\Lambda > 0$ propagates downstream with the CF wave speed and represents the eigendisturbance of the boundary layer.
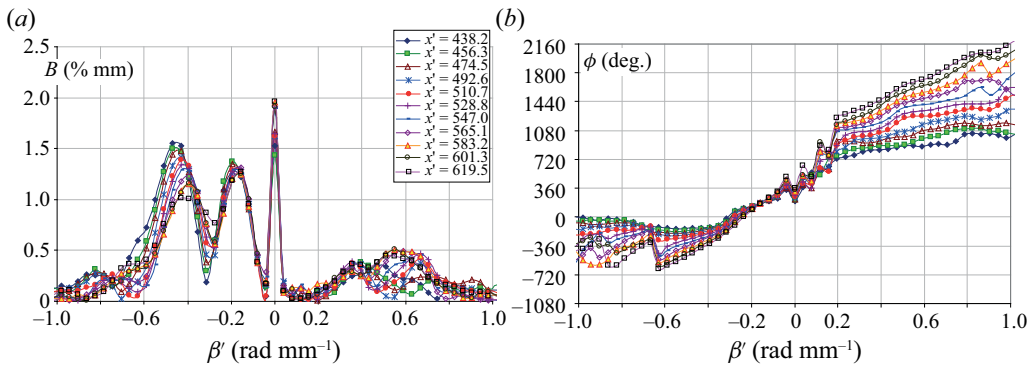
FIGURE 1. Example of downstream evolution of amplitude (*a*) and phase (*b*) parts of spanwise-wavenumber spectra of distributedly excited boundary-layer disturbances measured at $U/U_e = 0.6$ at frequency $f = 24.59$ Hz. DR experiment.

The situation is very different if the efficiency function is negative ($\Lambda < 0$, (2.21)). The newly produced portion of the CF wave cancels completely the previous portion and generates, in addition, a new CF wave. The phase of the remaining portion of disturbance $[\phi_v(x' + \Delta x'_b/2) + \lambda_v^d(x' + \Delta x'_b/2)]$ corresponds to the phase of the CF wave excited anew in the point $x' + \Delta x'_b/2$. This phase is equal, in fact, to the freestream vortex phase $\phi_v(x' + \Delta x'_b/2)$ (modified by the receptivity function phase $\lambda_v^d(x' + \Delta x'_b/2)$). In case when the receptivity phase λ_v^d is independent of x' the disturbance observed in the boundary layer at $\Lambda < 0$ propagates downstream with the freestream vortex speed. This is a bounded disturbance rather than the eigendisturbance of the boundary layer. In fact, the CF wave production is absent in this case.

3. Downstream evolution of disturbance spectra

3.1. *Evolution of boundary-layer disturbance spectra in DR and S experiments*

The spanwise-wavenumber spectra shown in figures 1(*a,b*) and 2(*a,b*) represent two examples of the results of spatial Fourier decomposition of spanwise distributions of disturbance amplitudes and phases obtained in the boundary layer in DR experiments (i.e. for CF waves excited by freestream vortices in a distributed way) and in S experiments (i.e. for pure CF waves excited by the point source) for one of studied frequencies ($f = 24.59$ Hz). Each figure shows spectral amplitudes (panels *a*) and phases (panels *b*) for all 11 studied chordwise positions in the range $x' = 438.2$–619.6 mm ($x_c = 483.5$–683.5 mm with step of 20 mm). (The spectral phases here (as well as in figure 3) correspond to a non-Cartesian (x_c, z'_c)-coordinate system, that is, they are calculated for the position of the z'-coordinate origin on the x-axis (i.e. at $z = 0$).)

The normalisation of the spectral amplitudes B corresponds to the Fourier integral taken from the measured amplitudes A as a percentage (without $1/(2\pi)$ in front of the integral) with dimensional dz' (in millimetres), that is, not normalised by the local boundary-layer displacement thickness, which is close to 1 mm and increases slowly downstream; see figure 8 in Part 1 (Borodulin *et al.* 2021). Note, however, that the spectral amplitude normalisation does not affect the DR coefficients because this normalisation is the same for the spectra of the freestream vortices (B_v) and for those of the excited instability waves (B^d), as in the present study (see (2.8)).
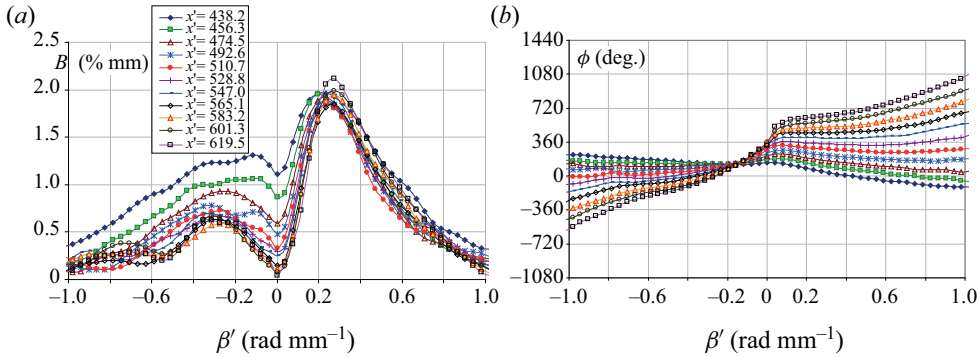
FIGURE 2. Example of downstream evolution of amplitude (*a*) and phase (*b*) parts of spanwise-wavenumber spectra of pure CF waves excited by a point source. Here $U/U_e = 0.6$, $f = 24.59$ Hz. S experiment.
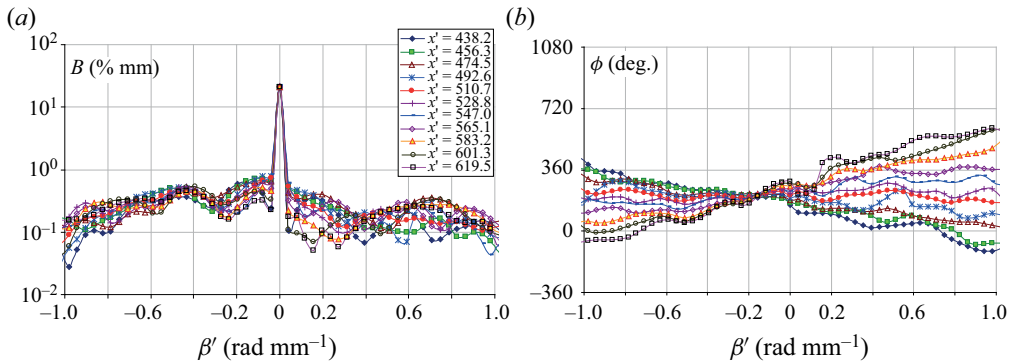

FIGURE 3. Example of downstream evolution of amplitude (*a*) and phase (*b*) parts of spanwise-wavenumber spectra of freestream vortices measured at $y = \delta$. Here $f = 24.59$ Hz. DR experiment.

The spectra of the boundary-layer perturbations distributedly excited in DR experiments (figure 1) are qualitatively similar. The amplitude spectra display four main maxima, two located at negative spanwise wavenumbers, one at $\beta' = 0$ (the quasi-two-dimensional mode) and one (or two sometimes) at positive spanwise wavenumbers in a range that is close to the most amplified CF instability modes. As was mentioned in §5.3 of Part 1 (Borodulin *et al.* 2021), some rather significant spatial beatings of spectral amplitudes and phases are observed in several spanwise-wavenumber ranges indicating the presence of the distributed generation of CF waves. However, in the range of small negative spanwise wavenumbers (around $\beta' = -0.1$ to -0.2 rad mm^{-1}) the spectral amplitudes depend very weakly on the chordwise coordinate (if any) despite these modes attenuating rapidly for pure CF waves measured in the S experiment (see figure 2*a*). As shown in the following, this range corresponds to a resonant distributed excitation of CF waves (see §§3.3 and 4).

The spectra of pure CF waves obtained in the S experiment for various chordwise locations (such as those shown in figure 2) look rather simpler to each other. The CF modes with negative spanwise wavenumbers attenuate mainly, whereas those with the spanwise

wavenumbers around 0.5 rad mm^{-1} display weak amplification (excluding one of two first spatial points, as discussed in § 3.3).

The spectra obtained in DR and S experiments at two other studied frequencies ($f = 34.88$ and 44.78 Hz) are qualitatively similar to those shown in figures 1 and 2 and just described previously.

3.2. *Spanwise-wavenumber spectra of freestream vortices at $y = \delta$ (DR experiments)*

Figure 3 shows an example of a set of the spanwise-wavenumber spectra obtained at $y = \delta$ from the spanwise distributions of amplitudes and phases of the streamwise component of velocity fluctuations in the freestream vortex at one of studied frequencies ($f = 24.59$ Hz). The amplitude spectra (figure 3a) are shown on a logarithmic scale due to the presence of a very large spectral component with $\beta' = 0$ associated with a quasi-two-dimensional vortex produced in the flow by a uniform part of the vibrating wire.

The amplitude spectra (figure 3a) obtained for a fixed frequency but at different chordwise positions do not display any strong streamwise evolution in contrast to the corresponding spectra obtained for the boundary-layer perturbations in the DR (figure 1a) and S (figure 2a) experiments. This feature indicates a nearly neutral streamwise behaviour of the vortex amplitudes at the boundary-layer edge, that can be explained by the competition between the vortex decay and movement of its centre towards the boundary-layer edge as seen in figure 16 in Part 1 (Borodulin *et al.* 2021).

The phase spectra (figure 3b) look relatively smooth in the whole studied spanwise-wavenumber range, excluding the vicinity of the quasi-two-dimensional mode with $\beta' = 0$. This observation is consistent with significantly different orientation of vorticity vectors for essentially three-dimensional and for quasi-two-dimensional freestream vortices (see Borodulin *et al.* (2021), and § 3.3 of the current paper).

The spectra of freestream vortices obtained in DR experiments for two other studied frequencies ($f = 34.88$ and 44.78 Hz) are qualitatively similar to those shown in figure 3.

3.3. *Increments and dispersion characteristics of pure CF waves and freestream vortices: possibility of resonant distributed excitation of CF modes*

The most important characteristics of downstream development of pure CF waves (S experiment) and freestream vortices (DR experiment), obtained after spanwise-wavenumber Fourier decomposition, are presented in figures 4–6 versus the spanwise wavenumber β' for all three studied frequencies. Panels (*a*) show the disturbance increments $-\alpha'_i$ (S experiment) and $-\alpha'_{vi}$ (freestream vortices in the DR experiment) in the x' direction; panels (*b*) display the streamwise wavenumbers α^*_r (S experiment) and α^*_{vr} (freestream vortices in the DR experiment) in the x^* direction; panels (*c*) present the disturbance phase velocities $C^*_x/U_{emean} = (\omega/\alpha^*_r)/U_{emean}$ (S experiment) and $C^*_{vx}/U_{emean} = (\omega/\alpha^*_{vr})/U_{emean}$ (freestream vortices in the DR experiment) in the x^* direction (where U_{emean} is the averaged boundary-layer edge velocity in the studied range of the streamwise coordinate, that is very close to U_e at $x_c = 583.5$ mm); finally, panels (*d*) show the disturbance propagation angles $\theta^* = \tan^{-1}(\beta^*/\alpha^*_r)$ (S experiment) and $\theta^*_v = \tan^{-1}(\beta^*/\alpha^*_{vr})$ (freestream vortices in the DR experiment).

The spatial increments and the streamwise wavenumbers were obtained in the following way. The streamwise distributions of the spectral amplitudes (normalised by local boundary-layer edge velocity) were approximated by exponents with the help of the least-squares fit method, whereas the corresponding distributions of spectral phases were
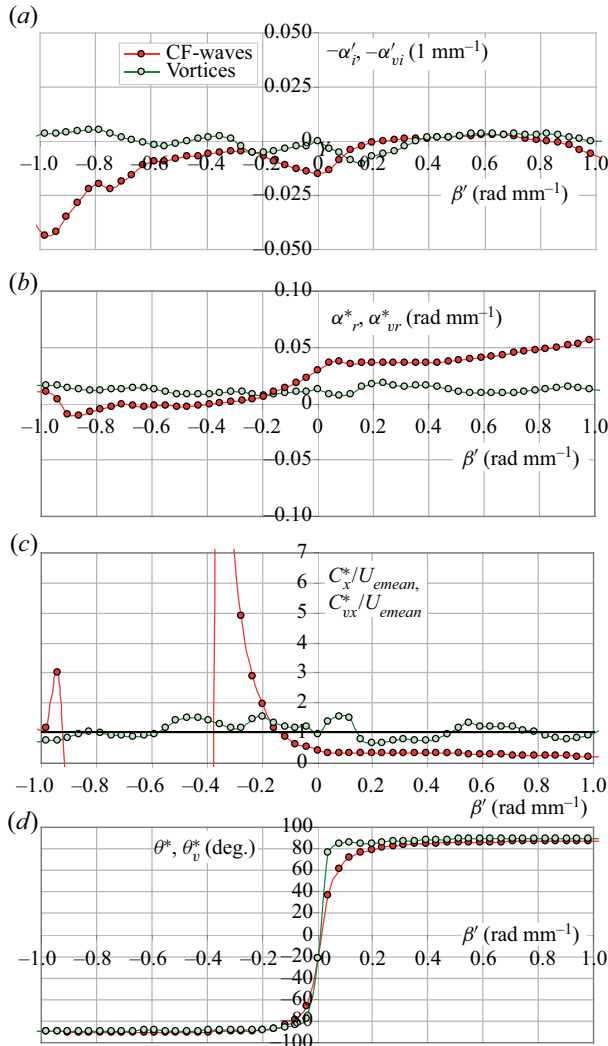
FIGURE 4. Comparison of the most important characteristics of downstream development of pure CF waves (S experiment) and freestream vortices (DR experiment), obtained after spanwise-wavenumber Fourier decomposition: (*a*) increments, (*b*) streamwise wavenumbers, (*c*) phase velocities and (*d*) wave-propagation angles. Here $f = 24.59$ Hz.

approximated by straight lines. Note, that in most cases, the approximations looked very well indicating that the deviations from the exponential behaviour of spectral amplitudes and from the linear behaviour of spectral phases were rather weak in the studied range of the chordwise coordinate. However, when performing this procedure for pure CF wave (S experiment), the first spatial point (or first two points) were usually omitted because these points were too close to the point source and the spectral amplitudes decayed in this region very quickly owing to the influence of the disturbance source near-field and/or of an admixture of rapidly attenuating Tollmien–Schlichting (TS) waves, which were also excited by the source.
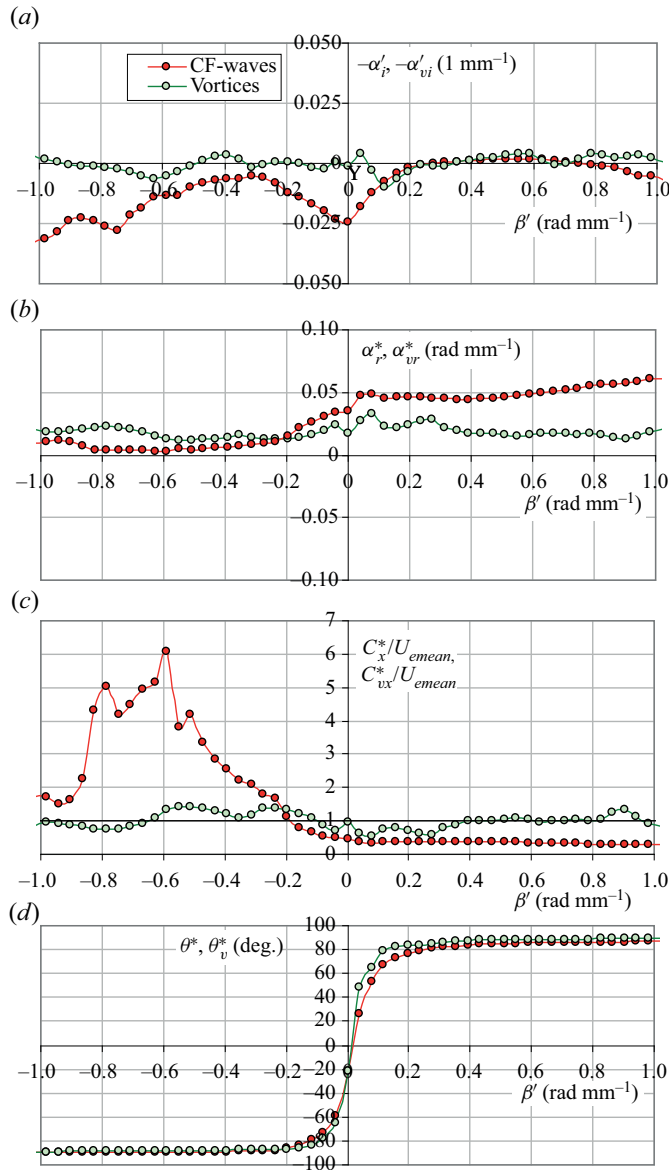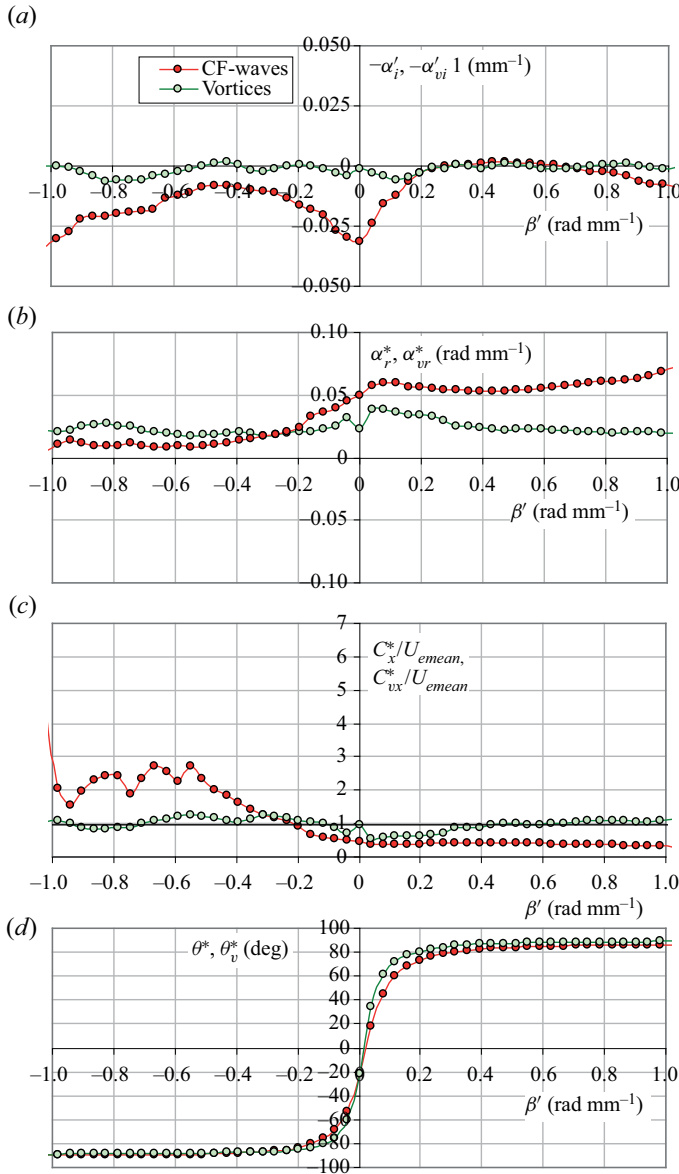
FIGURE 5. Comparison of the most important characteristics of downstream development of pure CF waves (S experiment) and freestream vortices (DR experiment), obtained after spanwise-wavenumber Fourier decomposition: (*a*) increments, (*b*) streamwise wavenumbers, (*c*) phase velocities and (*d*) wave-propagation angles. Here $f = 34.88$ Hz.

The increments presented in figures 4(*a*), 5(*a*) and 6(*a*) display a rather typical behaviour of the normal CF waves, similar to that observed previously by Gaponenko, Ivanov & Kachanov (1995*a,b*) at rather similar experimental conditions (at a somewhat lower freestream speed). At the lowest studied frequency ($f = 24.59$ Hz) the increments $-\alpha'_i$ of pure CF modes are positive in the spanwise wavenumber range $\beta' \approx$ 0.21–0.8 rad mm^{-1}. This range narrows when the frequency increases and is reduced to

(a)

(b)

(c)

(d)

FIGURE 6. Comparison of the most important characteristics of downstream development of pure CF waves (S experiment) and freestream vortices (DR experiment), obtained after spanwise-wavenumber Fourier decomposition: (a) increments, (b) streamwise wavenumbers, (c) phase velocities and (d) wave-propagation angles. Here $f = 44.78$ Hz.

$\beta' \approx 0.25$–0.65 rad mm^{-1} at the highest studied frequency ($f = 44.78$ Hz). All other CF modes decay downstream. The fastest attenuation is observed for quasi-two-dimensional modes (with β' around zero) and for very large negative values of the spanwise wavenumbers. The attenuation rates increase usually with frequency.

The freestream vortex increments $-\alpha'_{vi}$ (measured at the boundary-layer edge) oscillate with β' around zero. At some spanwise wavenumbers they are negative, at others they

are positive. Their values depend also on the frequency excluding mode with $\beta' = 0$ (i.e. the quasi-two-dimensional vortex produced by the uniform part of the vibrating wire), the increment of which is equal to zero almost exactly at all frequencies.

Figures 4(*b*), 5(*b*) and 6(*b*) show the dispersion functions for CF modes $\alpha_r^*(\beta', f)$ and for freestream vortices $\alpha_{vr}^*(\beta', f)$. The CF mode curves are again rather similar to those found in previous experiments. The streamwise wavenumbers α_r^* increase with β' for all frequencies and approach the axis $\alpha_r^* = 0$ at negative values of the spanwise wavenumber. At the lowest studied frequency (figure 4*b*), α_r^* oscillate around zero at $\beta' \leq -0.3$ approximately. The dispersion curves for freestream vortices display, in contrast, nearly constant streamwise wavenumber $\alpha_{vr}^*(\beta', f)$, the average of which value depends, however, on frequency. The sense of this value is clarified in figures 4(*c*), 5(*c*) and 6(*c*) where the streamwise velocities are shown. The freestream vortices propagate downstream, on average, with the freestream speed independently of frequency. This result is consistent with the physical sense. Note, however, that the streamwise wavenumbers and phase speeds of different spectral modes are somewhat different. This fact is probably conditioned by the rather complicated spatial shapes of the excited three-dimensional vortices, which change downstream and by the varying displacement of the vortex spectral components in the wall-normal direction when moving downstream.

The dispersion curves presented in figures 4(*b,c*), 5(*b,c*) and 6(*b,c*) demonstrate the possibility of the resonant distributed excitation of CF waves by freestream vortices. Indeed, the resonance of wavenumbers appears in the distributed vortex receptivity problem when for a given value of the spanwise wavenumber $\beta' = \beta'_{res}$, the streamwise-wavenumber detuning is $\sigma'_r(\beta'_{res}) = \alpha'_{gvr}(\beta'_{res}) - \alpha'_r(\beta'_{res}) = \alpha'_{gr}(\beta'_{res}) + \alpha'_{vr}(\beta'_{res}) - \alpha'_r(\beta'_{res}) = 0$ (see § 2.1). Under the assumption that the DR phase $\lambda_v^d(x')$ is constant (i.e. $\alpha'_{gr} = 0$), the resonance of wavenumbers is observed when $\alpha'_{vr}(\beta'_{res}) = \alpha'_r(\beta'_{res})$. This relationship is equivalent to $\alpha_{vr}^*(\beta'_{res}) = \alpha_r^*(\beta'_{res})$ and means just coincidence of the wavevectors of pure CF modes and freestream vortex modes in the point of crossing the corresponding dispersion curves (leading, in particular, to $C_{vx}^*(\beta'_{res}) = C_x^*(\beta'_{res})$ and $\theta_v^*(\beta'_{res}) = \theta^*(\beta'_{res})$). Figures 4(*b,c*), 5(*b,c*) and 6(*b,c*) show that such crossing is really observed for all frequencies studied. This happens in a narrow range of negative spanwise wavenumbers $\beta' \approx \beta'_{res}$; the value of β'_{res} decreases with frequency and is equal approximately to -0.18, -0.24 and -0.29 rad mm^{-1} for frequencies $f = 24.59$, 34.88 and 44.78 Hz, respectively.

Note, that the non-resonant solutions (2.11) and (2.14) remain valid for the resonance of wavenumbers described previously if the increment detuning $\sigma'_i(\beta'_{res}) = \alpha'_{gvi}(\beta'_{res}) - \alpha'_i(\beta'_{res}) = \alpha'_{gi}(\beta'_{res}) + \alpha'_{vi}(\beta'_{res}) - \alpha'_i(\beta'_{res}) \neq 0$. However, if $\sigma'_i(\beta'_{res})$ is also equal to zero, these solutions do not work and only the resonant solution (2.12) can be used for approximation of the experimental data. Under the assumption that the complex-valued DR amplitude $\bar{G}_v^d(x')$ is constant (i.e. $\alpha'_{gi} = \alpha'_{gr} = 0$), the true resonance (i.e. the resonance of complex-valued wavenumbers) can be observed only when $\alpha_{vr}^*(\beta'_{res}) = \alpha_r^*(\beta'_{res})$ and simultaneously $\alpha_{vi}^*(\beta'_{res}) = \alpha_i^*(\beta'_{res})$. This condition is not satisfied exactly in the present experiments although a tendency to its satisfaction is observed in a range of small negative spanwise wavenumbers β' (see figures 4*a,b*–6*a,b*).

Meanwhile, under the assumption that the DR amplitudes and phases are variable in the chordwise direction (i.e. when $\alpha'_{gi} \neq 0$ and/or $\alpha'_{gr} \neq 0$), the satisfaction of the true resonance condition ($\bar{\sigma}' = 0$) can be checked only after obtaining the experimental receptivity functions because the values of $\alpha'_{gr}(\beta')$ and $\alpha'_{gi}(\beta')$ are unknown at the present stage of the data processing. Therefore, sometimes (in some suspected cases) we also used
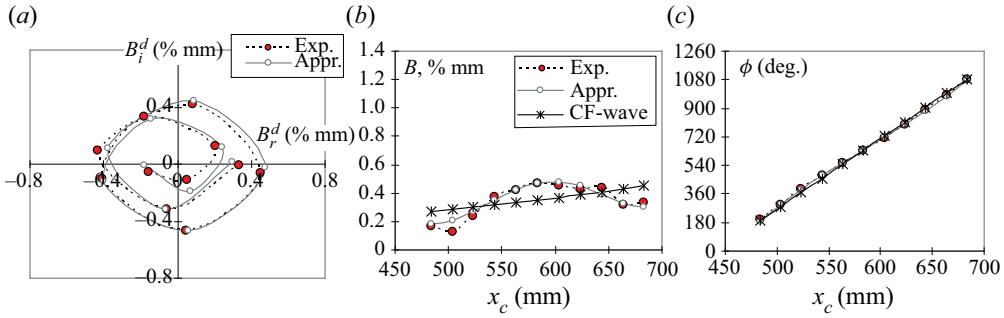
FIGURE 7. Example of the evolution of characteristics of a distributedly excited CF mode with $f = 24.59$ Hz, $\beta' = +0.668$ rad mm^{-1} in DR experiments and their approximations by non-resonant analytical solution (2.14) in comparison with the evolution of a pure CF mode extracted from the results of DR measurements by means of approximation. Approximation is made for case $\bar{G}_v^d(x') = $ const.

the approximation of our experimental data by the resonant analytical solution (2.12). This point is discussed in § 4.2.

The disturbance propagation angles presented in figures 4(*d*), 5(*d*) and 6(*d*) show that almost all investigating perturbations (both inside and outside the boundary layer) have very large inclination angles of their wavevectors to the x^*-axis, which exceed mainly the absolute values of 80° (excluding several points around $\beta' = 0$). At $\beta' > \beta'_{res}$, the absolute values of the freestream vortex propagation angles θ_v^* are greater than those of the CF wave propagation angles θ^*, whereas at $\beta' < \beta'_{res}$ they are lower, although the difference between these two angles is rather small.

4. Distributed vortex receptivity functions

4.1. *Examples of the approximation of experimental data by analytical solutions*

4.1.1. *Approximation for constant receptivity coefficients*

Several examples of results of approximation of distributions $\bar{B}^d(x_c)$ measured in DR experiments by non-resonant analytical solution (2.14) are given in figures 7–10 for frequency $f = 24.59$ Hz for four different values of the spanwise wavenumber β': +0.668, +0.314, −0.157 and −0.471 rad mm^{-1}, respectively. (Note that figures 7–10, as well as figures 11–16, correspond to the results obtained in a non-Cartesian coordinate system (x_c, z_c') because of its convenience for illustration, although the final approximations have been performed in the Cartesian coordinate system (x', z'). This circumstance influences only the spectral phases.) Panels (*a*) show the results of the approximation of experimental trajectories in the plane of complex-valued amplitudes (B_r^d, B_i^d) (where the x_c coordinate plays the role of a variable parameter), whereas panels (*b,c*) demonstrate the corresponding results of approximation for streamwise distributions of spectral amplitudes $B^d(x_c)$ and phases $\phi^d(x_c)$, respectively. Closed (red) circles in all panels show the measured values, while open (white) circles display the approximated values, which correspond to the analytical solution (2.14). Panels (*b*) and (*c*) contain, in addition, the streamwise distributions of amplitudes and phases, respectively, of pure CF waves extracted from the DR experimental distributions by means of the approximation procedure (the first terms in general solutions (2.11) and (2.14)).
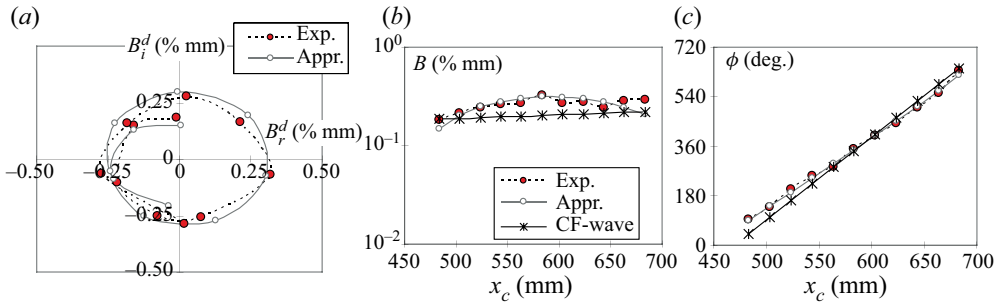
FIGURE 8. Example of the evolution of characteristics of a distributedly excited CF mode with $f = 24.59$ Hz, $\beta' = +0.314$ rad mm^{-1} in DR experiments and their approximations by non-resonant analytical solution (2.14) in comparison with the evolution of a pure CF mode extracted from the results of DR measurements by means of approximation. Approximation is made for case $\bar{G}_v^d(x') = $ const.
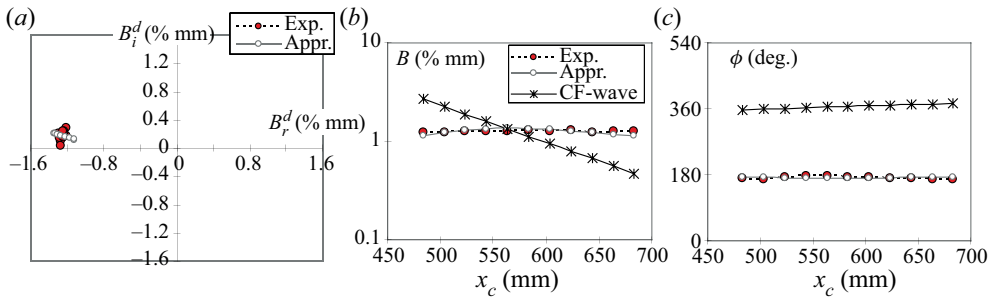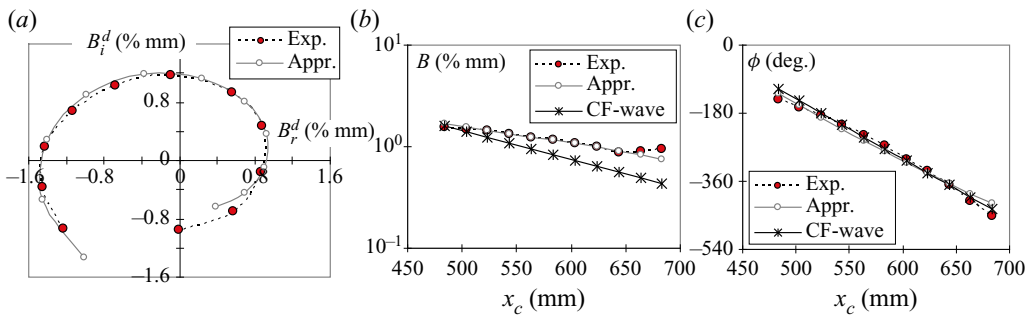

FIGURE 9. Example of the evolution of characteristics of a distributedly excited CF mode with $f = 24.59$ Hz, $\beta' = -0.157$ rad mm^{-1} in DR experiments and their approximations by non-resonant analytical solution (2.14) in comparison with the evolution of a pure CF mode extracted from the results of DR measurements by means of approximation. Approximation is made for case $\bar{G}_v^d(x') = $ const.

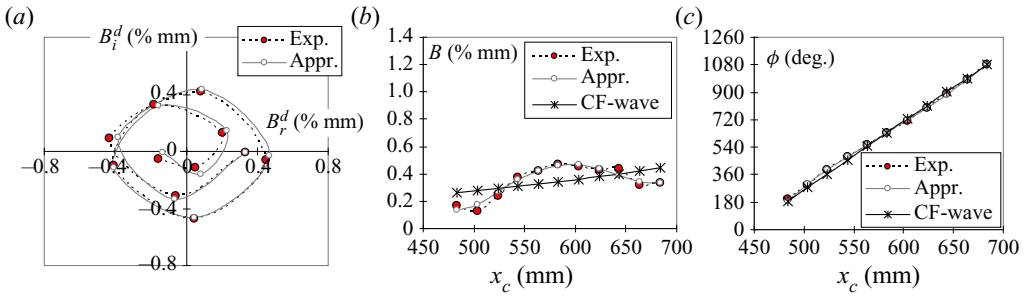FIGURE 10. Example of the evolution of characteristics of a distributedly excited CF mode with $f = 24.59$ Hz, $\beta' = -0.471$ rad mm^{-1} in DR experiments and their approximations by non-resonant analytical solution (2.14) in comparison with the evolution of a pure CF mode extracted from the results of DR measurements by means of approximation. Approximation is made for case $\bar{G}_v^d(x') = $ const.

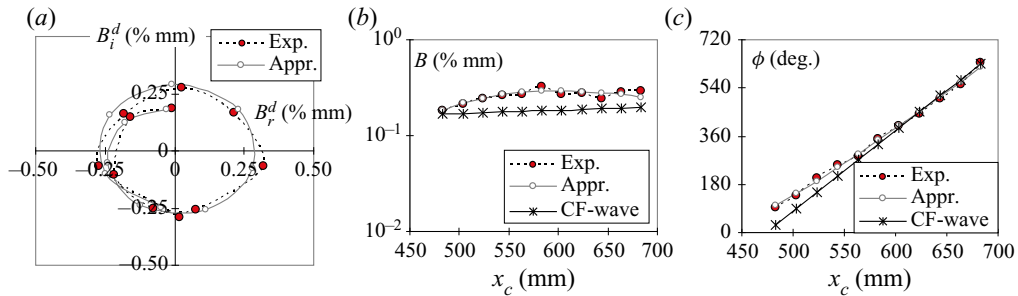FIGURE 11. Example of the evolution of characteristics of a distributedly excited CF mode with $f = 24.59$ Hz, $\beta' = +0.668$ rad mm^{-1} in DR experiments and their approximations by non-resonant analytical solution (2.11) in comparison with the evolution of a pure CF mode extracted from the results of DR measurements by means of approximation. Approximation is made for case $\bar{G}_v^d(x') \neq$ const.

FIGURE 12. Example of the evolution of characteristics of a distributedly excited CF mode with $f = 24.59$ Hz, $\beta' = +0.314$ rad mm^{-1} in DR experiments and their approximations by non-resonant analytical solution (2.11) in comparison with the evolution of a pure CF mode extracted from the results of DR measurements by means of approximation. Approximation is made for case $\bar{G}_v^d(x') \neq$ const.
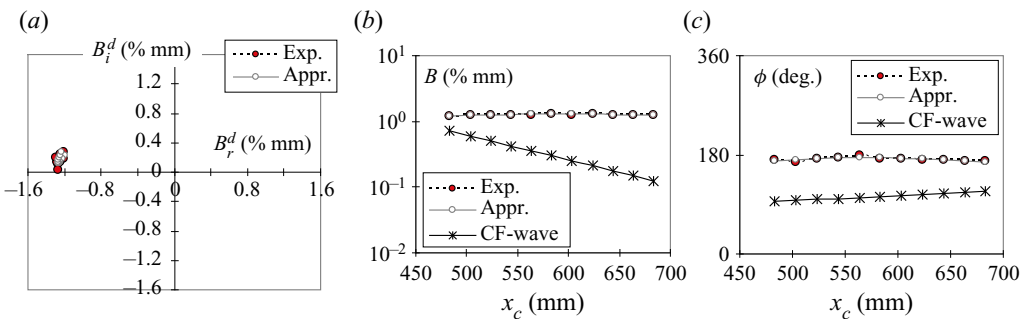

FIGURE 13. Example of the evolution of characteristics of a distributedly excited CF mode with $f = 24.59$ Hz, $\beta' = -0.157$ rad mm^{-1} in DR experiments and their approximations by non-resonant analytical solution (2.11) in comparison with the evolution of a pure CF mode extracted from the results of DR measurements by means of approximation. Approximation is made for case $\bar{G}_v^d(x') \neq$ const.
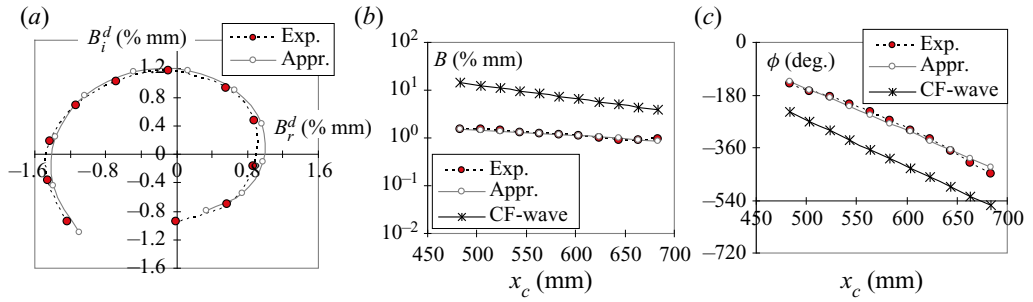
FIGURE 14. Example of the evolution of characteristics of a distributedly excited CF mode with $f = 24.59$ Hz, $\beta' = -0.471$ rad mm^{-1} in DR experiments and their approximations by non-resonant analytical solution (2.11) in comparison with the evolution of a pure CF mode extracted from the results of DR measurements by means of approximation. Approximation is made for case $\bar{G}_v^d(x') \neq$ const.

FIGURE 15. Example of the evolution of characteristics of a distributedly excited CF mode with $f = 24.59$ Hz, $\beta' = -0.157$ rad mm^{-1} in DR experiments and their approximations by resonant analytical solution (2.12) in comparison with the evolution of a pure CF mode extracted from the results of DR measurements by means of approximation. Approximation is made for case $\bar{G}_v^d(x') \neq$ const.
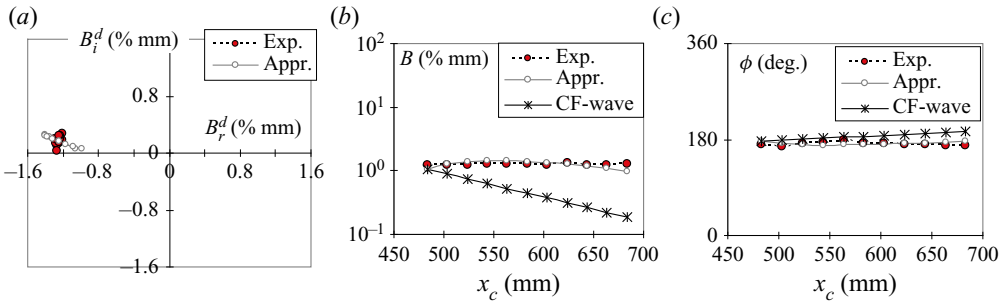

FIGURE 16. Example of the evolution of characteristics of a distributedly excited CF mode with $f = 24.59$ Hz, $\beta' = -0.471$ rad mm^{-1} in DR experiments and their approximations by resonant analytical solution (2.12) in comparison with the evolution of a pure CF mode extracted from the results of DR measurements by means of approximation. Approximation is made for case $\bar{G}_v^d(x') \neq$ const.

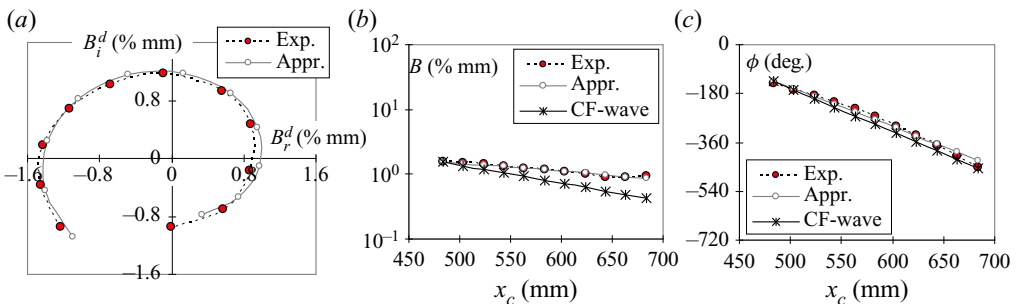The case $\beta' = -0.157$ rad mm^{-1} (figure 9) is very special, it is close to the resonance of the streamwise wavenumbers with $\sigma_r' = 0$ (see figure 4b) and, simultaneously, to the true resonance when $\sigma_i' = 0$ (see figure 4a). Figure 9(b) shows that in this case, the initial amplitude of the extracted CF wave seems to be predicted poorly, as does the initial phase (figure 9c). This is a sign that the approximation by the non-resonant solution with constant receptivity coefficient does not work sufficiently well at $\beta' = -0.157$ rad mm^{-1}.

4.1.2. *Approximation for variable receptivity coefficients*

The results presented in figures 11–14 correspond to those shown in figures 7–10 (again for frequency $f = 24.59$ Hz) but in the present case the approximations of the measured distributions are performed by a more general non-resonant analytical solution (2.11), which assumes the possibility of variation of the receptivity amplitude and phase with the chordwise coordinate. The approximation accuracy is better in all cases presented in figures 11–14 compared with those shown in figures 7–10. Therefore, one can assume that this approximation should give, in general, more accurate values of the receptivity amplitudes and phases. Note, however, that the influence of the experimental error on the result increases in the case of variable receptivity coefficients as well, that is, the method becomes more sensitive to the experimental error compared with the case of constant receptivity coefficients.

Despite the better accuracy of approximation reached in the present case (with variable $\bar{G}_v^d(x_c)$), the initial amplitudes and phases of the extracted CF wave are predicted poorly for the two shown negative values of the spanwise wavenumber with $\beta' = -0.157$ and -0.471 rad mm^{-1} (figures 13b,c and 14b,c). The amplitude at $\beta' = -0.157$ rad mm^{-1} seems to be underestimated (figure 13b), in contrast to the $\bar{G}_v^d(x') = $ const. case (figure 9b) where it was overestimated, whereas at $\beta' = -0.471$ rad mm^{-1} (figure 14b) it is strongly overestimated (by one order of magnitude), in contrast to the $\bar{G}_v^d(x') = $ const. case (figure 10b) where it was predicted reasonably well. Similar problems are seen for the initial CF wave phases (figures 13c and 14c). This is a sign that the approximation by the non-resonant solution with variable receptivity coefficient does not work properly at $\beta' = -0.157$ and -0.471 rad mm^{-1}.

4.1.3. *Approximation in resonant points*

Figures 15 and 16 show two examples of approximation of experimental distributions performed by means of the resonant analytical solution (2.12) at frequency $f = 24.59$ Hz for spanwise wavenumbers $\beta' = -0.157$ and -0.471 rad mm^{-1}, respectively. The main results of this resonant approximation look a bit worse for $\beta' = -0.157$ rad mm^{-1} (figure 15) than those obtained for the non-resonant case with variable $\bar{G}_v^d(x_c)$ (figure 13). However, the initial amplitude and phase of the extracted CF mode are now very realistic (figures 15b,c) in contrast to the two non-resonant approximations (figures 9b,c and 13b,c). A similar, very striking, difference is observed at $\beta' = -0.471$ rad mm^{-1} between the resonant case (figures 16b,c) and the non-resonant case for variable $\bar{G}_v^d(x_c)$ (figures 14b,c).

Thus, summarising the discussion presented in §§ 4.1.1–4.1.3, one can conclude that all three methods of data processing provide reasonably good approximation of the experimental distributions but have to be applied selectively for different values of the spanwise wavenumber (at each fixed disturbance frequency) in order to obtain values of all searching parameters with the best accuracy.
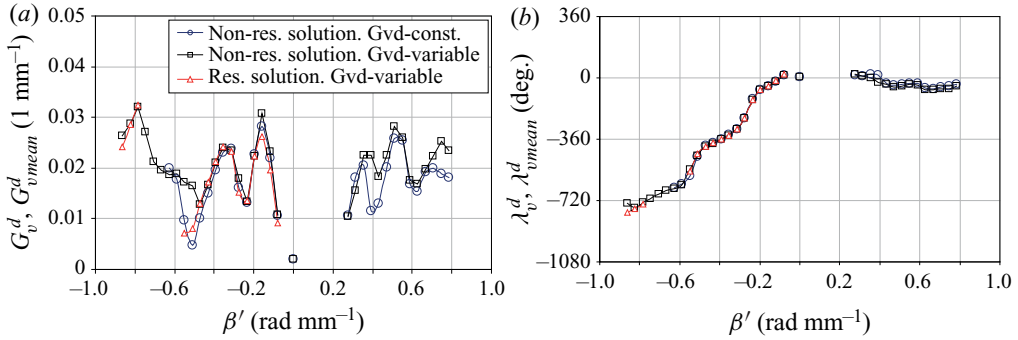
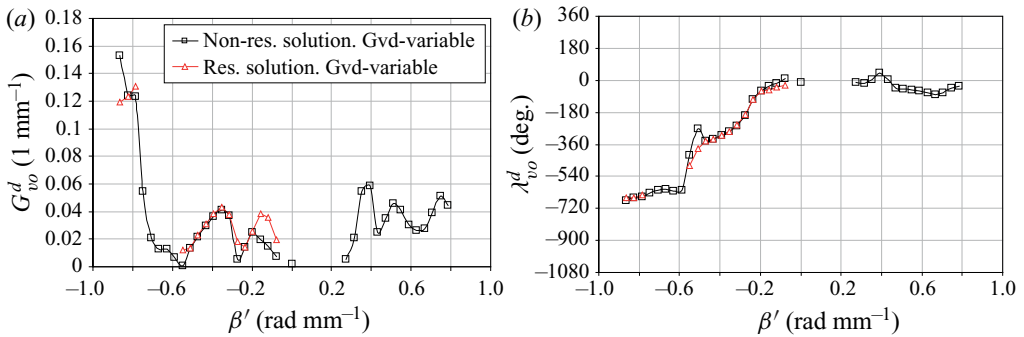FIGURE 17. Amplitudes (*a*) and phases (*b*) of DR coefficients for $f = 24.59$ Hz.

FIGURE 18. Initial amplitudes (*a*) and initial phases (*b*) of variable DR coefficients for $f = 24.59$ Hz.

4.2. *Receptivity coefficients*

The results of obtaining characteristics of the distributed vortex receptivity, based on the streamwise component of the freestream vortices (measured at the boundary-layer edge), are presented for frequency 24.59 Hz in figures 17–24 versus the spanwise wavenumber for cases of both constant and variable receptivity coefficients (functions). All values shown in these figures correspond to the (x', z')-coordinate system. Only those points are presented in these spectra, which were obtained with a reasonably good accuracy of approximation corresponding to values of the dispersion (2.15) less than 0.2 (except for figures 22a, displaying the dispersion functions for all cases, and for the distributions for $\bar{G}_v^d(x') = $ const. approximation shown in figures 21a,b and 22b, which are independent of the approximation results).

The receptivity amplitudes and phases obtained by means of three different kinds of approximation are shown in figures 17(*a,b*). The results obtained under assumption of variable receptivity coefficients (both in the non-resonant and resonant case) are presented in these figures by their mean values (G_{vmean}^d and λ_{vmean}^d) averaged in the chordwise range of the measurements. The corresponding initial (i.e. at $x' = 438.2$ mm) receptivity amplitudes and phases (G_{vo}^d and λ_{vo}^d) are shown in figures 18(*a,b*), respectively, whereas the receptivity-function increments ($-\alpha_{gi}'$) and chordwise wavenumbers (α_{gr}') are shown in figures 19(*a,b*).
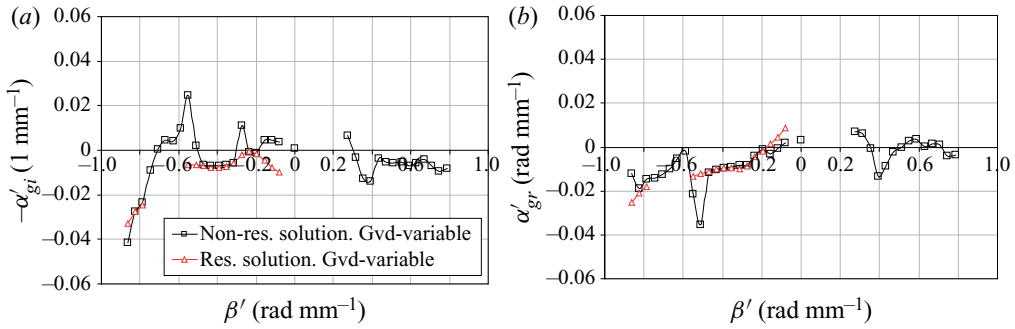
FIGURE 19. Spatial increments (*a*) and chordwise wavenumbers (*b*) of variable DR coefficients for $f = 24.59$ Hz.
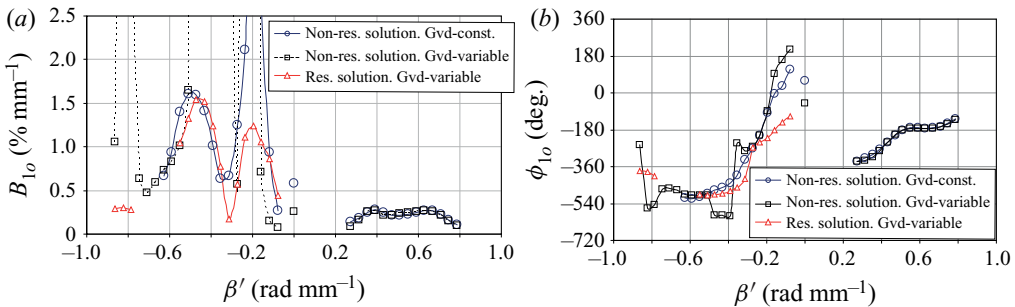

FIGURE 20. 'Initial' (at $x_c = 483.5$ mm) amplitudes (*a*) and phases (*b*) of excited CF waves evaluated by means of approximations for variable receptivity coefficients for $f = 24.59$ Hz.
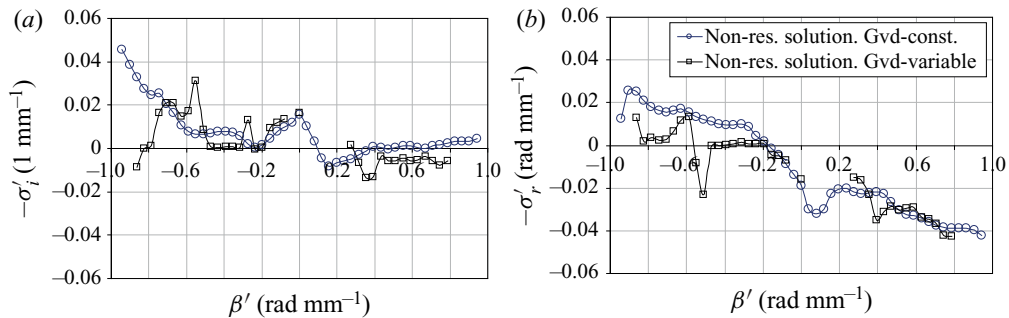
FIGURE 21. Resonant detunings of chordwise increments (*a*) and wavenumbers (*b*) for DR at $f = 24.59$ Hz.

The receptivity functions presented in figures 17(*a*,*b*) display a rather complicated dependence on the spanwise wavenumber, especially the amplitudes. At $\beta' < 0$, the receptivity amplitude distributions (figure 17*a*) have three maxima with phase jumps (close to 180°) between them in points of the amplitude minima (figure 17*b*). At small positive values of β' (approximately between points $+0.04$ and $+0.25$ rad mm^{-1}), the accuracy of the approximation is the lowest (see figure 22) because of very small amplitudes of
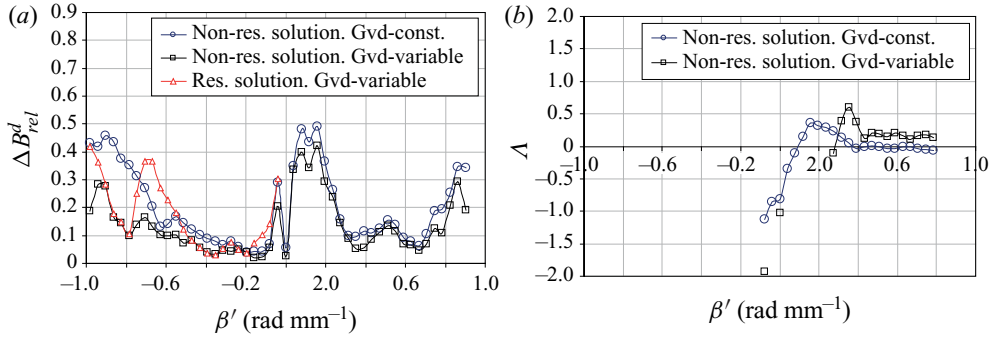
FIGURE 22. Dispersion of approximation (*a*) and efficiency function (*b*) for DR at $f = 24.59$ Hz.

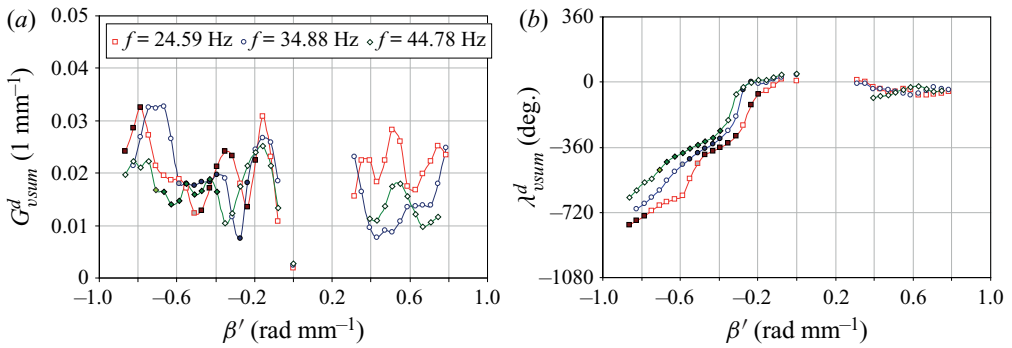

FIGURE 23. Summarised values of amplitudes (*a*) and phases (*b*) of DR coefficients for all studied frequencies: $f = 24.59$, 34.88 and 44.78 Hz.
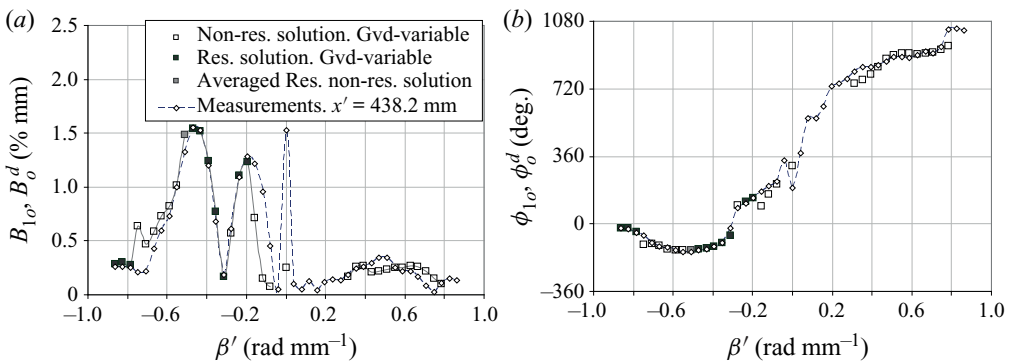

FIGURE 24. Comparison of amplitude (*a*) and phase (*b*) parts of initial (at $x_c = 483.5$ mm) spectra of excited CF modes measured directly and obtained from approximations for $f = 24.59$ Hz.

the boundary-layer perturbations measured in DR experiment (see figure 1a). Therefore, these points are absent in all figures. At $\beta' > +0.25$ there are three receptivity-amplitude maxima (figure 17a) with very small (if any) phase shifts between them (figure 17b).

The receptivity phase displays a very fast decrease with absolute value of the spanwise wavenumber at $\beta' < 0$ and a rather weak decrease (with subsequent flattening) at $\beta' > 0$ (figure 17b). The mean values of the receptivity amplitudes (figure 17a) obtained under the assumption of variable $\bar{G}_v^d(x')$ are rather similar, in general, to the amplitudes found under the assumption of its independence of the x' coordinate, especially in the ranges of the best accuracy of approximation (cf. figure 22a). The receptivity phases are practically the same in these two cases (figure 17b). The lowest receptivity amplitude (very close to zero) is observed for quasi-two-dimensional mode (with $\beta' = 0$). The receptivity there is lower than the maximum by a factor of 16. This result is consistent with the conclusion drawn in Part 1 (Borodulin *et al.* 2021) that the DR to streamwise aligned vortices is much stronger than to those with the spanwise orientation of the vorticity vector.

In the case of variable $\bar{G}_v^d(x')$, the receptivity increments $-\alpha'_{gi}$ (figure 19a) characterise the receptivity amplitude variation (growth or decay) in the chordwise direction. In the ranges of the best accuracy (at $\beta' \approx -0.5$ to -0.1 rad mm^{-1} and $\beta' \approx +0.3$ to $+0.7$ rad mm^{-1}, see figure 22a), they are mainly negative or close to zero. This result is consistent with the physical sense because the receptivity has to decrease slowly downstream due to thickening of the boundary layer. The receptivity coefficient streamwise wavenumbers α'_{gr} characterise the chordwise variation of the phase delay between the freestream vortices and the excited CF waves. They are mainly negative at $\beta' < 0$ (and decrease with absolute value of β') and mainly close to zero (constant receptivity phase) at $\beta' > 0$.

The results of extraction of pure CF modes, the first terms in general solutions (2.11) and (2.14), are presented in figures 20(a,b). The initial (i.e. at $x' = 438.2$ mm) amplitudes B_{1o} and phases ϕ_{1o} of these modes are shown there versus the spanwise wavenumber. (The corresponding increments and the streamwise wavenumbers of these modes are presented in figures 4a,b.) The shape of the amplitude spectra (figure 20a) looks qualitatively similar to that of the spectra directly measured in the boundary layer and presented in figure 1a. This is especially true in the range of positive spanwise wavenumbers. However, there are several important differences. First, the amplitude spectra extracted by means of the analytical approximations (figures 20a,b) do not have the large peak for the quasi-two-dimensional mode (at $\beta' = 0$) observed in directly measured spectra (figure 1a). In the case of a variable receptivity function, this peak is especially small. This result corresponds to a very low receptivity to the quasi-two-dimensional mode indicated previously (see figure 17a) and means that the disturbance observed in the boundary layer at this wavenumber represents mainly the bounded (forced) perturbation rather than the CF wave. Second, the height of the peak near $\beta' \approx -0.2$ rad mm^{-1} is much larger in figure 20(a) compared with that in figure 1(a) in the two non-resonant approximations (with both constant and variable $\bar{G}_v^d(x')$). The heights of two other peaks (near $\beta' \approx -0.45$ and -0.8 rad mm^{-1}) are also very much larger in the non-resonant approximation with variable $\bar{G}_v^d(x')$ (figure 20a) compared with those observed in figure 1(a). For example, the amplitude of the peak at $\beta' \approx -0.45$ rad mm^{-1} obtained in the case with variable receptivity coefficient is greater than that measured directly in the flow by a factor of approximately 17. This discrepancy (which was also discussed in § 4.1) indicates that the result of the approximations by the non-resonance solutions is not satisfactory in the vicinities of these peaks.

It was also found that the convergence of the approximation procedure is worse in the vicinity of the peaks discussed previously and the result of the approximation is more highly dependent on the initial values of the varying parameters. (In all cases the result with the smallest dispersion (2.15) had been finally selected.) Despite the spectra of the approximation accuracy (figure 22a) does not display any singularities in the vicinity of these peaks, the non-realistic amplitudes of them and the problems with the approximation indicate approaching the resonance discussed in § 3.2. Indeed, the spectra of the real (σ'_r) and imaginary $(-\sigma'_i)$ parts of the resonance detuning parameter $\bar{\sigma}'$ presented in figures 21(a) and 21(b), respectively, show that in the vicinity of $\beta' \approx -0.2$ rad mm^{-1}, the two quantities are close to zero both in the cases of constant and variable receptivity function. At the position of another peak (around $\beta' \approx -0.45$ rad mm^{-1}), the approximation for the case $\bar{G}^d_v(x') = $ const. is made at non-zero $\bar{\sigma}'$ (which is just equal to $\bar{\alpha}'_v - \bar{\alpha}'$ in this case and is independent of the result of the approximation) and, accordingly, the height of this peak in figure 21(a) is rather close to that directly measured (see figure 1a). However, in the case of the approximation with variable $\bar{G}^d_v(x')$, the values of both σ'_r and $-\sigma'_i$ are very close to zero in three regions: near $\beta' \approx -0.8, -0.45$ and -0.2 rad mm^{-1} (figures 21a,b). In these regions, the resonance again leads to the appearance of non-realistically large peaks seen in figure 20(a).

The third set of data presented in figures 17, 20 and 23 show the results of approximation by the resonant solution (2.12). This approximation was made only in the range of negative spanwise wavenumbers, where the detuning parameter $\bar{\sigma}'$ is more or less close to zero or can be close to zero (see figure 21a,b). The approximation by the resonant solution does not change very much the receptivity amplitudes and phases (figure 17) in those points where the approximation dispersion is smaller than, or close to, that reached in the non-resonant case (see figure 22). The same is true for the initial receptivity amplitudes and phases (figure 18) and for the receptivity-coefficient increments and streamwise wavenumbers (figure 19). The most dramatic changes are observed in the spectra of initial amplitudes (figure 20a) and phases (figure 20b) of the CF wave extracted from the boundary-layer perturbations. Indeed, the large-amplitude peaks, found around $\beta' \approx -0.8$, -0.45 and -0.2 rad mm^{-1} in cases of application of the non-resonant approximations, disappear and the amplitudes in the vicinity of these peaks become realistic (figure 20a) and very close to those measured directly in the boundary layer (see figure 1a).

Let us finally consider the efficiency function Λ (2.22). In the present case this function has a clear physical sense only in the range of positive spanwise wavenumbers, where the excitation is far from the resonance itself (when $\bar{\sigma}' = 0$) and from the resonance of wavenumbers (when $\sigma'_r = 0$) (see figure 21). The spanwise-wavenumber distributions of this function are presented in figure 22(b) for cases of non-resonant approximations with constant and variable receptivity coefficients. In the case of constant-$\bar{G}^d_v(x')$ approximation, the value of Λ is independent of the result of approximation and depends only on characteristics of the pure CF modes and the freestream vortices. In this case Λ is positive only around $\beta' \approx 0.2$ and close to zero or negative for other values of the spanwise wavenumber. This means that the efficiency of the distributed excitation of the most amplified CF waves (around $\beta' \approx 0.4$–0.75 rad mm^{-1}) is close to zero (in the absence of any surface non-uniformities) in a sense that a portion of disturbance excited at $x' = x'_1$ is completely cancelled by another portion excited at $x' = x'_1 + \pi/|\sigma'_r|$ (see § 2.3). However, in the case of variable-$\bar{G}^d_v(x')$ approximation, the values of Λ are positive in a broad range of spanwise wavenumbers at $\beta' > 0.3$ rad mm^{-1}. (In this case Λ depends on the results of approximation.) Rather similar results are obtained for two other studied frequencies ($f = 34.88$ and 44.78 Hz). In particular, the efficiency function Λ is found to

be always positive in the range of spanwise wavenumbers $\beta' \approx 0.45\text{--}0.75$ rad mm^{-1} in all cases of variable-$\bar{G}_v^d(x')$ approximations.

The summarised main results, obtained for frequency $f = 24.59$ Hz, are presented in figures 23 and 24 for the receptivity coefficients and for the initial spectrum of extracted CF waves, respectively. The points shown in these figures correspond mainly to those with the lowest values of dispersion (2.15) among all three kinds of approximations used. Note that at all frequencies, the approximations performed for constant receptivity coefficients gave always higher dispersion than those carried out for variable $\bar{G}_v^d(x')$ (either the non-resonant or resonant ones). For several points shown in figures 23 and 24, the resonant solutions with a bit higher dispersion have been chosen when they gave a better reconstruction of the CF wave initial spectrum but close values of the receptivity amplitudes and phases. The resonant points are marked with black symbols. Grey points (one in every plot) indicate a wavenumber, at which the results obtained for the resonant and non-resonant approximations have been averaged. The receptivity amplitudes $G_{vsum}^d(\beta')$ and phases $\lambda_{vsum}^d(\beta')$ are compared in figure 23(a) with those determined for two other frequencies ($f = 34.88$ and 44.78 Hz), whereas the initial spectrum of the extracted CF wave ($B_{1o}(\beta')$ and $\phi_{1o}(\beta')$) is compared in figure 24 with the spectrum of boundary-layer perturbations ($B_o^d(\beta')$ and $\phi_o^d(\beta')$) measured directly in the experiment (i.e. with the first spectrum shown in figure 1). (Recall that for the resonant points, the values of $B_{1o}(\beta')$ and $\phi_{1o}(\beta')$ do not exist and they are replaced by equivalent, in this case, values of $B_o^d(\beta')$ and $\phi_o^d(\beta')$ obtained from the resonant approximations.)

Figure 24 shows that, in contrast to figure 20, the initial CF wave spectrum, extracted mainly by means of the least dispersion approximations (including the resonant ones), is very similar to that measured directly. These two spectra should not coincide with each other, but their closeness indicates the successfulness of application of the used approximation procedure.

All results presented in this section for frequency of 24.59 Hz and discussed previously turned out to be qualitatively very similar to those obtained for two other frequencies studied: $f = 34.88$ and 44.78 Hz. Therefore, we skip the description for these frequencies except for the DR functions presented in figure 23.

4.3. *General analysis of experimentally obtained DR characteristics*

Thus, the distributed vortex receptivity functions are obtained and the CF waves are extracted from the boundary-layer perturbations. Several issues appear in connection with these experimental results. These issues are concentrated around the main question: 'How can we explain the behaviour and properties of the receptivity coefficients obtained and of the CF waves observed?'

4.3.1. *Beatings of receptivity functions*

One of the most intricate questions is associated with the cause of such complicated dependencies of the receptivity amplitudes and phases on the spanwise wavenumber, observed in all studied cases. This cause is not clear at present. It is definitely clear that the spanwise-wavenumber beatings of the receptivity amplitudes and phases do not appear due to experimental error. It is also difficult to believe that such complicated behaviour corresponds to the physics of the DR. (Nature usually 'prefers' nice and simple distributions.) A possible explanation of the observed complicated behaviour is as follows. One can assume that the definition of the distributed vortex receptivity function based on the streamwise component of the freestream vortices, measured at the

boundary-layer edge, is not optimal and does not correspond properly to the physics of the receptivity mechanism under study.

There are several other possible definitions of the DR coefficients, which can be based, for instance, on v- or w-components of velocity fluctuations in the freestream vortices measured at the boundary-layer edge. Alternatively, a certain combination of the disturbance velocity vector components (such as one of the vorticity vector components) could play the predominant role in the CF wave distributed excitation. Moreover, we can assume that some the other parts of the freestream vortices located farther from the boundary-layer edge could also play an important role in the CF wave distributed excitation. These questions remain unanswered at present and need a theoretical analysis, which cannot be performed in our experimental group. However, we have carried out special measurements and analysis in order to estimate the DR characteristics based on the assumption about a predominant role of either the v- or w-component of velocity fluctuations in the freestream vortices measured at the boundary-layer edge. The obtained results did not look better than those discussed previously obtained based on the u-component of the freestream vortices.

It is also necessary to note here that there is no correlation between the receptivity amplitude spectra and the presence (or absence) of the receptivity resonances; neither for the true spectra (when $\sigma_r = \sigma_i = 0$) or the resonances of streamwise wavenumbers (when $\sigma_r = 0$ but $\sigma_i \neq 0$). Thus, the receptivity amplitude beatings cannot be explained by the presence of the resonances. This observation correlates with the physical sense because the DR coefficient is an essentially local (in the x' direction) characteristic of the flow (see the definition given by (2.8) and (2.9)), whereas the resonance occurs only in a range of the streamwise coordinate. In other words, the DR coefficients characterise the efficiency of local excitation in every spatial point, whereas the resonance provides a phase coordination of the CF waves excited at different chordwise locations.

4.3.2. *Frequency dependence of receptivity functions*

Let us analyse now the frequency dependence of the DR amplitudes and phases. Owing to the complicated spanwise-wavenumber beatings of the receptivity amplitudes, observed for all studied frequencies, the frequency distributions for different fixed values of the spanwise wavenumber are very complicated as well and do not show any clear tendencies. Therefore, we analyse the receptivity-amplitude frequency distributions using several kinds of averaging along the spanwise-wavenumber axis. The results are presented in figure 25(*a*).

The quasi-two-dimensional mode (with $\beta' = 0$) is unique and averaging has not been performed for it. Despite the receptivity amplitudes being very low for this mode, they increase with frequency monotonously in an almost linear way (with a growth rate remaining, however, very low). In contrast, the receptivity amplitudes averaged for all positive spanwise wavenumbers ($\beta' > 0$) decrease with frequency. They drop quite significantly in the range between 24.59 and 34.88 Hz and decrease much less at the next step (between 34.88 and 44.78 Hz). The receptivity amplitudes averaged in the range of large negative spanwise wavenumbers $-0.86 \leq \beta' \leq -0.51$ rad mm^{-1} (with values of $|\beta'|$ greater then those of the two main peaks) display growth at the first frequency step but decay at the second one. Meanwhile, the averaging performed in the range $-0.51 \leq \beta' < 0$ rad mm^{-1}, which includes the two large receptivity peaks, shows a monotonous, almost linear decay. Almost the same result is observed when the averaging is made for all measured values of the spanwise wavenumber (except for $\beta' = 0$).
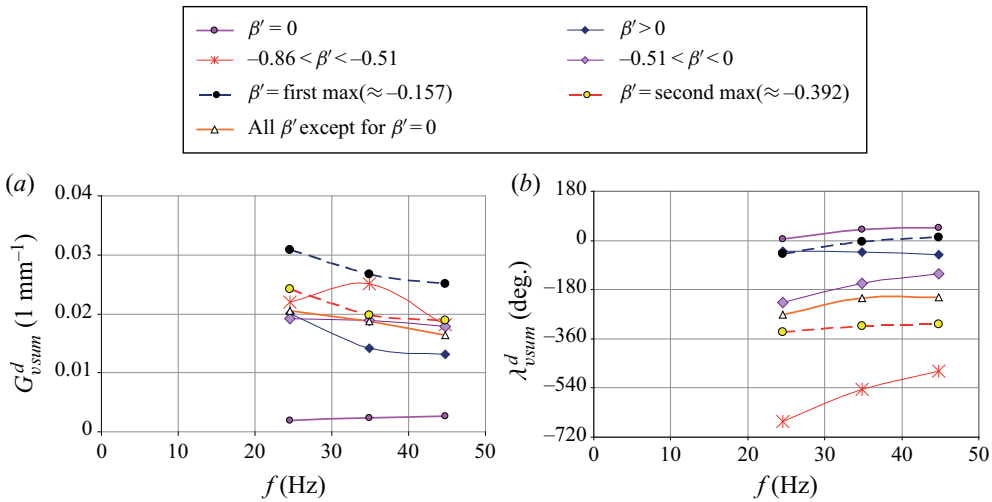
FIGURE 25. Estimated frequency dependencies of distributed vortex receptivity amplitudes (*a*) and phases (*b*) averaged in several spanwise-wavenumber ranges.

In addition, the frequency dependence of heights of two main receptivity-amplitude peaks, located around $\beta' \approx 0.15$ and 0.38 rad mm^{-1}, is also presented in figure 25(*a*). These distributions show a weak decay of the receptivity with frequency. Thus, we can conclude that, in general, the distributed vortex receptivity amplitudes depend very weakly on frequency with a tendency to their reduction. Note that this result is quite different from the previous result obtained for the three-dimensional localised surface-vibration receptivity by Gaponenko *et al.* (2002) for almost the same swept-wing boundary layer, where the receptivity was enhanced with frequency very significantly (in a linear way). In two other experiments devoted to the localised vortex receptivity of the same swept-wing boundary layer due to scattering of freestream vortices on surface roughness (Borodulin *et al.* 2013) and on surface vibrations (Borodulin *et al.* 2016), the receptivity amplitudes always grow with frequency. In the former case, this was a quasi-linear growth with frequency of freestream vortices $f_{vor} = f_{CF}$, whereas in the latter case this was either quasi-linear growth with frequency of the excited CF modes f_{CF}, or a quasi-exponential growth with frequency of surface vibrations f_{sur} and with the coefficient $k = f_{sur}/f_{vor}$ characterising the degree of non-stationarity of the surface non-uniformity.

The corresponding frequency distributions of the DR phases are presented in figure 25(*b*). The averaging was performed in the same spanwise-wavenumber ranges as for the receptivity amplitudes. It is seen that the receptivity phases increase with frequency in all spanwise-wavenumber ranges except for $\beta' > 0$, where they remain almost constant (with a slight tendency to decrease). The latter behaviour is similar to that found by Gaponenko *et al.* (2002) for the three-dimensional localised surface-vibration receptivity (in the whole rage of the spanwise wavenumbers), whereas the former is different but similar to that found in another experiment devoted to the localised receptivity due to scattering of freestream vortices on surface roughness (Borodulin *et al.* 2013). Note also that the behaviour of the distributed vortex receptivity phases in the range of negative spanwise wavenumbers is almost the same as that found for the quasi-two-dimensional mode ($\beta' = 0$).

4.3.3. *Causes of excitation of CF waves with negative and positive β'*

The physical nature of the most powerful perturbations observed in the swept-wing boundary layer at negative spanwise wavenumbers (around $\beta' \approx -0.25$ and -0.5 rad mm^{-1} (see, e.g., figures 1*a* and 24*a*) has become clear after the data processing performed in the present work. Note, first, that the receptivity amplitude maxima do not coincide with these peaks in all studied cases and, hence, cannot be explained by a larger receptivity at the wavenumbers corresponding to these peaks. The analysis has shown that these large peaks correspond to CF waves resonantly excited by the distributed vortex receptivity mechanism found in the present experiments. Despite the corresponding pure CF modes attenuate downstream, the presence of the resonant DR mechanism forces them to be amplified starting from rather small values of the chordwise coordinates (upstream the region of main measurements, i.e. at $x' < 438.2$ mm). To provide this amplification the resonance of the streamwise wavenumbers ($\sigma'_r = 0$) is enough, that is, the equality $\sigma'_i = 0$, required additionally for the true (full) resonance, is not necessary.

It is important to note that the regular linear stability theory enables, in fact, the description of the disturbance amplitude behaviour in the ranges of the spanwise wavenumbers where the resonant excitation of the CF waves occurs (see, e.g., figure 15*b*). Thus, the CF wave growth in these ranges is governed by the mechanism of the resonant distributed vortex receptivity rather than by the linear stability mechanism. From the physical viewpoint, the growth of the CF waves in these β' ranges (always with negative spanwise wavenumbers) is similar, in a certain sense, to the 'transient growth' observed in bypass transition scenarios at high turbulence levels, because the boundary-layer disturbances appear due to the direct influence of the freestream vortices. However, in the present case this growth is not transient (at least when either $\bar{\sigma}'$ or σ'_r is exactly equal to zero), not 'non-modal' and, consequently, it is not necessary to attract the 'lift-up' effect to explain this growth.

The physical nature of the boundary-layer disturbances observed at positive spanwise wavenumbers is significantly different. Indeed, the resonant DR is absent in this range (in the case of the absence of any significant surface roughness). As was shown in §2.3, the non-resonant distributed excitation of CF waves can be efficient (on a smooth surface) only if the efficiency function $\Lambda = \sigma'_i/|\sigma'_r|$ is positive. In this case, the distributed generation can occur due to: (i) a weak natural streamwise non-uniformity of the boundary layer (which can lead to $-\alpha'_{gi} < 0$), (ii) a weak streamwise non-uniformity of the freestream vortices (which can have an increment $-\alpha'_{vi} < 0$, i.e. to decay) and/or (iii) the boundary-layer instability (i.e. when $-\alpha'_i > 0$). The experimental results discussed in §4 have shown that $-\alpha'_{vi} \approx 0$, on average, in the present case. Meanwhile, the receptivity amplitudes decay usually (in the case of variable $\bar{G}^d_v(x')$) in the range of positive spanwise wavenumbers β' (i.e. $-\alpha'_{gi} < 0$ mainly) and the pure CF waves mainly grow downstream (i.e. $-\alpha'_i > 0$) in the range $\beta' \approx 0.3$–0.7 rad mm^{-1}. These circumstances lead to small but mainly positive values of the efficiency function Λ (and, similarly, to positive values of $\sigma'_i = \alpha'_{gi} + \alpha'_{vi} - \alpha'_i$) observed in a broad range of positive spanwise wavenumbers, indicating that the CF wave excitation is efficient. Thus, one can conclude that the CF waves with positive spanwise wavenumbers appear in the boundary layer mainly due to the non-resonant distributed vortex receptivity mechanism. At the present experimental conditions, this mechanism is much less efficient than the resonant one and, therefore, the amplitudes of the extracted CF waves are much lower here compared with those observed at negative spanwise wavenumbers near the resonant points.

4.3.4. *Possible role of distributed surface roughness in excitation of CF waves*

Let us now discuss the role of the distributed surface roughness in the CF wave generation due to the distributed vortex receptivity. In the case of the resonant excitation of CF modes occurred in the range of $\beta' < 0$ this role seems to be very minor. A low-amplitude distributed roughness is able only to provide a streamwise modulation of the receptivity process, to destroy locally (a little bit) the resonant phase relationships between the newly and previously excited CF waves but it cannot accelerate the resonant CF wave excitation occurring on a smooth surface. Therefore, one can expect that the roughness barely influences the transition position when it is initiated by the resonantly amplified CF modes with negative spanwise wavenumbers.

A completely different situation is observed in the range of positive spanwise wavenumbers. The non-resonant distributed CF wave excitation is rather weak there. The roughness is able to intensify it significantly by means of 'conversion' of the non-resonant distributed excitation to the resonant one (see, e.g., Borodulin *et al.* (2004, 2006), for the cases of distributed excitation of TS waves by freestream vortices in a two-dimensional boundary layer). This conversion can be provided by the surface roughness with the resonant streamwise wavenumbers $\alpha'_{sr}(\beta') = \sigma'_r(\beta')$, where $2\pi/\sigma'_r(\beta')$ is the period of spatial beatings of the excited boundary-layer perturbations in the streamwise direction. The values of resonant detunings of the streamwise wavenumbers $\sigma'_r(\beta')$ have been found experimentally in the present work for every studied frequency for cases of constant and variable receptivity coefficients (see, e.g., §4.2 and figure 21b). For positive spanwise wavenumbers between $+0.3$ and $+0.7$ rad mm^{-1} values of $\sigma'_r(\beta')$ vary from 0.02 to 0.06 rad mm^{-1} and correspond to the chordwise periods of the most dangerous, resonant roughness between approximately 300 and 100 mm. These large-scale surface disturbances correspond to surface waviness rather than to surface roughness. Smaller scales of the waviness could promote excitation of only linearly stable CF modes, which have very large spanwise wavenumbers (greater than approximately 0.8 rad mm^{-1}), whereas the longer scales of the roughness could help in the excitation of CF modes with either very small spanwise wavenumbers (which also always attenuate downstream) or with negative, non-resonant spanwise wavenumbers; but this excitation can hardly be stronger than the resonant excitation on smooth surface discussed previously.

4.3.5. *Distributed vortex receptivity and transition prediction methods*

The predominant influence of the resonant DR on the CF mode growth in the range of negative spanwise wavenumbers must be taken into account when designing the transition prediction methods based on the linear stability theory and the linear receptivity theory. It is possible, in principle, that the perturbations amplified by the resonant distributed vortex receptivity mechanism could be able to lead to transition (if their amplitudes reach a nonlinear threshold). In this case the transition can not be predicted by either the *N*-factor method or the variable *N*-factor method because in such a case (hypothetical, at present) the resonant distributed vortex receptivity mechanism plays the predominant role and this mechanism must be incorporated into the transition prediction approach, which aims to take into account the influence of the freestream turbulence on the swept-wing laminar–turbulent transition. In the case of a smooth surface, a generalised advanced method of prediction of transition initiated by travelling CF waves seems to have to include two criteria of transition working in parallel and based on ideas of: (i) the distributed linear receptivity with the linear stability (as in the variable *N*-factor method); and (ii) the resonant DR (which incorporates the effects of linear stability). The first scenario

leads to the variable *N*-factor approach with a slight modification, which would take into account the spatial beatings of the boundary-layer disturbances, which can be significant if the disturbance amplitude reaches a nonlinear threshold of secondary instability at one of amplitude peaks of the beatings. Meanwhile, the second scenario leads to an amplitude method of transition prediction, because: (i) the disturbance growth is not described in this case by the linear stability theory; and (ii) the transition can occur even if the initial CF wave amplitude (at branch I) is equal to zero. Such an advanced (combined) transition prediction method is absent at present.

5. Summary and concluding remarks

Thus, the data obtained in the S and DR experiments described in Part 1 (Borodulin *et al.* 2021) and devoted to the distributed vortex receptivity of a swept-wing boundary layer, have been deeply processed and discussed in the present paper (Part 2).

The following most important work has been performed. A detailed procedure of obtaining the distributed vortex receptivity coefficients (functions), based on approximation of the experimental data by non-resonant and resonant analytical solutions of the evolutionary equation, has been developed and applied.

The spatial Fourier decomposition of disturbance distributions, obtained for all kinds of disturbances has been performed. The downstream evolution of the spanwise-wavenumber spectral amplitudes and phases has been obtained for three kinds of perturbations: (i) the freestream vortices at the boundary-layer edge (DR experiments); (ii) the CF modes excited by them in a distributed way (DR experiments); and (iii) pure CF waves excited by a point source in the absence of the freestream vortices (S experiments).

Based on the analysis of spectral mode dispersion characteristics for freestream vortices (DR experiment) and for pure CF waves (S experiment), as well as on investigation of kinematic conditions, the possibility of a direct resonant distributed generation of CF waves by essentially three-dimensional freestream vortices (on smooth surface) has been found.

The distributed vortex receptivity characteristics have been found in Fourier space as functions of the spanwise-wavenumber and frequency. The receptivity characteristics have been obtained in both non-resonant and resonant cases under the assumptions that the receptivity is: (i) independent of the streamwise coordinate (in the studied range) and (ii) variable. All results have been analysed and compared.

In the case of constant receptivity coefficients (in the streamwise direction) the obtained receptivity characteristics include: (i) the receptivity amplitudes and phases; (ii) the initial amplitudes and phases of the upstream excited CF waves extracted from boundary-layer perturbations; (iii) the receptivity resonance detuning functions $\bar{\sigma}'(\beta')$, which include the chordwise periods of beatings $|\sigma'_r(\beta')|$, associated with the resonant period of surface roughness; and (iv) the efficiency functions $\Lambda(\beta')$. In the case of variable receptivity coefficients, the obtained receptivity characteristics include: (i) the initial receptivity amplitudes and phases; (ii) the average (in the streamwise range of measurements) receptivity amplitudes and phases; (iii) the receptivity-function increments and streamwise wavenumbers; (iv) the initial amplitudes and phases of the excited upstream CF waves extracted from boundary-layer perturbations; (v) the receptivity resonance detuning functions $\bar{\sigma}'(\beta')$, which include the chordwise periods of beatings $|\sigma'_r(\beta')|$ associated with the resonant period of surface roughness; and (vi) the efficiency functions $\Lambda(\beta')$.

The following most important results have been obtained.

(i) It has been found that the CF waves, which are predominant in the spanwise-wavenumber spectrum, have negative spanwise wavenumbers (i.e. propagate in the CF direction) and are excited basically due to the resonant distributed vortex receptivity mechanism. The increments of these CF waves do not correspond to the linear stability theory and the CF waves can be present in the boundary layer even if their initial amplitudes (at branch I of the neutral stability curve) are equal to zero. Meanwhile, the CF waves, which are the most amplified by the linear instability mechanism and have positive spanwise wavenumbers (i.e. propagate upstream of the CF), are excited due to the corresponding non-resonant distributed vortex receptivity mechanism and, therefore, their amplitudes are weaker usually compared with the resonantly generated CF waves.

(ii) A comparison of three different definitions of the distributed vortex receptivity function has shown that the definition based of the u-velocity component of the freestream vortex disturbance (measured at the boundary-layer edge) gives the most reasonable results, especially for negative spanwise wavenumbers compared with the definitions based on the v- and w-velocity components.

(iii) The vortex receptivity amplitudes (averaged in the studied chordwise range) turned out to have a very complicated (peaky) dependence on the spanwise wavenumber (especially at negative spanwise wavenumbers). The receptivity amplitudes, averaged in several spanwise-wavenumber ranges, display their very weak dependence on the vortex frequency with a tendency of a reduction.

(iv) It has been found that the receptivity to quasi-two-dimensional freestream vortices (with $\beta' = 0$, i.e. with predominance of the spanwise vorticity) is very much (many times) weaker than that to the essentially three-dimensional vortices (with predominance of the streamwise vorticity). This fact has been observed for all studied frequencies.

(v) The vortex receptivity phases have been found to decrease quickly with absolute value of the spanwise wavenumber at $\beta' < 0$ and remain almost constant at $\beta' > 0$ for all studied frequencies. The receptivity phases, averaged in several spanwise-wavenumber ranges, display their growth with the vortex frequency at negative and zero spanwise wavenumbers and have approximately neutral behaviour at positive spanwise wavenumbers.

(vi) The case of variable (in the chordwise direction) receptivity coefficients seems to correspond better to the DR mechanism under study because it provides a better accuracy of the experimental data approximation. The receptivity amplitudes decreases mainly downstream with increments $-\alpha'_{gi} \approx -0.005$ to -0.01 mm^{-1} (which seem to be weakly dependent on the frequency) excluding small absolute values of the spanwise wavenumber (approximately at $|\beta'| < 0.3$ rad mm^{-1}) where the increments are mainly close to zero. The receptivity phases decrease mainly downstream at negative spanwise wavenumbers below -0.3 rad mm^{-1}, increase at positive spanwise wavenumbers for frequency $f = 34.88$ Hz and remain mainly constant for other spanwise wavenumbers and frequencies.

(vii) In the range of positive spanwise wavenumbers, the detuning parameter of the wavenumber resonance σ'_r is always far from zero and negative, providing the spatial beatings of the boundary-layer perturbations distributedly excited by freestream vortices. The period of beatings is equal to $2\pi/|\sigma'_r|$, depends weakly on the frequency and increases with β'. The values of the efficiency function Λ obtained

experimentally have shown that the non-resonant excitation is mainly efficient ($\Lambda > 0$) in the range of $\beta' \approx 0.45$–0.75 rad mm^{-1}.

(viii) The periods of spatial beatings obtained experimentally provide us with the chordwise scales of the resonant surface roughness, which is able to 'convert' the non-resonant distributed excitation of CF waves into the resonant one. This conversion is especially important for the range of positive spanwise wavenumbers (including the range of the CF waves, which are the most amplified by the linear instability mechanism), where the distributed excitation occurred on the smooth surface is the non-resonant one.

Summarising the results of the measurements and analysis, the following most important conclusions can be drawn.

(*a*) The swept-wing boundary layer is much more distributedly receptive to essentially three-dimensional (i.e. streamwise elongated) vortices (in which the streamwise vorticity dominates) compared with quasi-two-dimensional vortices (with almost spanwise orientation of vorticity vectors).

(*b*) In contrast to the acoustic receptivity and the vortex receptivity of two-dimensional boundary layers, the distributed vortex receptivity of low-speed (incompressible) swept-wing boundary layers can be resonant even in the absence of any significant base-flow and surface non-uniformities.

(*c*) The largest amplitudes of the CF waves generated by the DR mechanism can be reached at negative spanwise wavenumbers (owing to the presence of the streamwise-wavenumber resonance), that is, for the waves, which are not the most amplified by the linear CF instability mechanism. The variable N-factor method of transition prediction cannot be applied in this case and an amplitude method of transition prediction has to be developed instead, which would be based on both linear stability and linear DR approaches.

(*d*) The small-amplitude distributed surface waviness seems to be unimportant for the distributed excitation of CF waves by freestream vortices in the range of negative spanwise wavenumbers (i.e. for waves propagated in the CF direction) owing to the strong resonant character of this excitation. However, such waviness seems to have a significant influence on the non-resonant distributed excitation, observed in the range of the CF waves most amplified by the linear-instability mechanism (propagated upstream the CF). It would be very desirable to check the correctness of this important conclusion in special experiments with application of controlled distributed surface waviness.

Declaration of interests

The authors report no conflict of interest.

REFERENCES

BORODULIN, V. I., IVANOV, A. V. & KACHANOV, Y. S. 2010*a* Distributed receptivity of swept-wing boundary layer to streamwise vortices. Part. 1. Experimental approach. In *XV International Conference on Methods of Aerophysical Research. Proceedings* (ed. V. M. Fomin), pp. 1–10. Institute of Theoretical and Applied Mechanics.

BORODULIN, V. I., IVANOV, A. V. & KACHANOV, Y. S. 2010*b* Distributed receptivity of swept-wing boundary layer to streamwise vortices. Part. 2. Receptivity characteristics. In *XV International Conference on Methods of Aerophysical Research. Proceedings* (ed. V. M. Fomin), pp. 1–10. Institute of Theoretical and Applied Mechanics.

BORODULIN, V. I., IVANOV, A. V., KACHANOV, Y. S. & FEDENKOVA, A. A. 2004 Distributed boundary-layer receptivity to non-stationary vortical disturbances with wall-normal vorticity in the presence of surface roughness. *Thermophys. Aeromech.* **11** (3), 355–390.

BORODULIN, V. I., IVANOV, A. V., KACHANOV, Y. S. & FEDENKOVA, A. A. 2007 Three-dimensional distributed receptivity of a boundary layer to unsteady vortex disturbances. In *XIII International Conference on Methods of Aerophysical Research (ICMAR 2007). Proceedings. Part III* (ed. V. M. Fomin), pp. 45–50. Parallel.

BORODULIN, V. I., IVANOV, A. V., KACHANOV, Y. S. & KOMAROVA, V. Y. 2006 Distributed two-dimensional boundary-layer receptivity to non-stationary vortical disturbances in the presence of surface roughness. *Thermophys. Aeromech.* **13** (2), 183–208.

BORODULIN, V. I., IVANOV, A. V., KACHANOV, Y. S. & ROSCHEKTAYEV, A. P. 2013 Receptivity coefficients at excitation of cross-flow waves by free-stream vortices in the presence of surface roughness. *J. Fluid Mech.* **716**, 487–527.

BORODULIN, V. I., IVANOV, A. V., KACHANOV, Y. S. & ROSCHEKTAYEV, A. P. 2016 Receptivity coefficients at excitation of cross-flow waves due to scattering of free-stream vortices on surface vibrations. *J. Fluid Mech.* **793**, 162–208.

BORODULIN, V. I., IVANOV, A. V., KACHANOV, Y. S. & ROSCHEKTAYEV, A. P. 2021 Distributed vortex receptivity of swept-wing boundary layer. Part 1. Efficient excitation of CF-modes. *J. Fluid Mech.* **908**, A14.

GAPONENKO, V. R., IVANOV, A. V. & KACHANOV, Y. S. 1995*a* Experimental study of a swept-wing boundary-layer stability with respect to unsteady disturbances. *Thermophys. Aeromech.* **2** (4), 287–312.

GAPONENKO, V. R., IVANOV, A. V. & KACHANOV, Y. S. 1995*b* Experimental study of cross-flow instability of a swept-wing boundary layer with respect to traveling waves. In *Laminar-Turbulent Transition* (ed. R. Kobayashi), pp. 373–380. Springer.

GAPONENKO, V. R., IVANOV, A. V., KACHANOV, Y. S. & CROUCH, J. D. 2002 Swept-wing boundary-layer receptivity to surface non-uniformities. *J. Fluid Mech.* **461**, 93–126.

KACHANOV, Y. S., BORODULIN, V. I., IVANOV, A. V. & ROSCHEKTAYEV, A. P. 2002*a* Distributed receptivity of swept-wing boundary layer to streamwise free-stream vortices. Part 1. Experimental procedure and primary results of measurements. *Tech. Rep.* Interim Project Report on Agreement No 106 (Exhibit 106I, Part A), June 2002. Institute of Theoretical and Applied Mechanics.

KACHANOV, Y. S., BORODULIN, V. I., IVANOV, A. V. & ROSCHEKTAYEV, A. P. 2002*b* Distributed receptivity of swept-wing boundary layer to streamwise free-stream vortices. Part 2. Structure of vortices and receptivity characteristics. *Tech. Rep.* Final Project Report on Agreement No 106 (Exhibit 106I, Part A), November 2002. Institute of Theoretical and Applied Mechanics.

WÜRZ, W., HERR, S., WAGNER, S. & KACHANOV, Y. S. 2002 A first experimental approach to the distributed 3D-vortex receptivity of a boundary layer on an airfoil. In *XI International Conference on Methods of Aerophysical Research. Proceedings. Part II*, pp. 173–178. Institute of Theoretical and Applied Mechanics.